IMA Journal of Applied Mathematics (2015) **80**, 1776–1798
doi:10.1093/imamat/hxv015
Advance Access publication on 26 June 2015

Characterizing the shape and material properties of hidden targets from magnetic induction data

Paul D. Ledger*
College of Engineering, Swansea University, Singleton Park, Swansea SA2 8PP, UK
*Corresponding author: p.d.ledger@swansea.ac.uk

and

William R. B. Lionheart
School of Mathematics, University of Manchester, Alan Turing Building, Oxford Road, Manchester M13 9PL, UK

[Received on 6 October 2014; revised on 13 April 2015; accepted on 31 May 2015]

The aim of this paper is to show that, for the eddy current model, the leading order term for the perturbation in the magnetic field, due to the presence of a small conducting magnetic inclusion, can be expressed in terms of a symmetric rank 2 polarization tensor. This tensor contains information about the shape and material properties of the object and is independent of position. We apply a recently derived asymptotic formula for the perturbed magnetic field, due to the presence of a conducting inclusion, which is expressed in terms of a new class of rank 4 polarization tensors (Ammari, H., Chen, J., Chen, Z., Garnier, J. & Volkov, D. (2014) Target detection and characterization from electromagnetic induction data. *J. Math. Pures Appl.*, **101**, 54–75.) and show that their result can be written in an alternative form involving a symmetric rank 2 tensor involving 6 instead of 81 complex components in an orthonormal coordinate frame. For objects with rotational and mirror symmetries we show that the number of coefficients is still smaller. We include numerical examples to demonstrate that the new polarization tensors can be accurately computed by solving a vector-valued transmission problem by *hp*-finite elements and include examples to illustrate the agreement between the asymptotic formula describing the perturbed fields and the numerical predictions.

Keywords: polarization tensors; asymptotic expansions; eddy currents; *hp*-finite elements; metal detectors; land mine detection.

1. Introduction

There is considerable interest in being able to locate and characterize conducting objects from measurements of mutual impedance between a transmitting and a receiving coil, where the coupling is inductive rather than due to the propagation of radio waves. The most obvious examples are in metal detection, where the goal is to identify and locate a highly conducting object in a low conducting background and applications include security screening, archaeological searches, maintaining food safety as well as for land mine clearance and the detection of unexploded ordnance (UXO). There is also considerable interest in being able to produce conductivity images from multiple magnetic induction measurements, most notably in magnetic induction tomography for medical applications (Griffiths, 2005; Zolgharni *et al.*, 2009) and industrial applications (Gaydecki *et al.*, 2000; Soleimani *et al.*, 2007). Furthermore, eddy current sensing techniques are also commonly used for the monitoring and defect detection in steel structures such as oil pipe lines and containment vessels as well as

monitoring corrosion of steel reinforcement bars in concrete structures such as bridges and buildings (Simmonds & Gaydecki, 1999).

The detection of land mines presents a huge challenge, the United Nations estimates that 'there are more than 110 million active mines [...] scattered in 68 countries with an equal number stockpiled around the world waiting to be planted' and that 'every month over 2000 people are killed or maimed by mine explosions (United Nations, 1997). Although metal detectors offer a portable means of detection current techniques are often not able to distinguish between benign and dangerous targets and, therefore, there is great interest in technological advancements that might increase the speed at which mines could be detected and increase safety.

By considering the time harmonic regime, and denoting the electric field intensity vector by $\boldsymbol{E}$ and the corresponding magnetic field intensity vector by $\boldsymbol{H}$, Somersalo *et al.* (1992) compute the Fréchet derivative of the Dirichet to Neumann (DtN) map with respect to small changes in permeability, permittivity and conductivity, $\delta\mu$, $\delta\epsilon$ and $\delta\mu$, respectively, in a bounded domain Ω and obtain

$$\int_{\partial\Omega} \hat{\boldsymbol{n}} \cdot (\boldsymbol{E} \times \boldsymbol{H}_0^* - \boldsymbol{E}_0^* \times \boldsymbol{H})\, \mathrm{d}S = \int_{\Omega} (\mathrm{i}\omega\delta\mu \boldsymbol{H}_0 \cdot \boldsymbol{H}_0^* - \mathrm{i}\omega\delta\epsilon \boldsymbol{E}_0 \cdot \boldsymbol{E}_0^* + \delta\sigma \boldsymbol{E}_0 \cdot \boldsymbol{E}_0^*)\, \mathrm{d}\Omega + O((\delta\mu, \delta\epsilon, \delta\sigma)^2),$$

as the parameter perturbations go to zero, where ω is the angular frequency, $(\boldsymbol{E}_0, \boldsymbol{H}_0)$ and $(\boldsymbol{E}_0^*, \boldsymbol{H}_0^*)$ are pairs of unique solutions to the unperturbed problem (i.e. plane wave solutions) and $\boldsymbol{E} := \boldsymbol{E}_0 + \delta\boldsymbol{E}$, $\boldsymbol{H} := \boldsymbol{H}_0 + \delta\boldsymbol{H}$ denote the solutions to the Maxwell system using the perturbed parameters. However, this is different to the situation of interest in the present work, which concerns the field perturbations due to the presence of an inclusion with a large conductivity contrast compared to the background medium.

For a bounded domain, Ammari *et al.* (2001) have obtained the corresponding asymptotic formula that describes the perturbation of the DtN map, which, when particularized for the case of single small inclusion with parameters μ_*, ϵ_* and σ_* located at $\boldsymbol{z}$, has a leading order term that can be expressed in terms of $\boldsymbol{w}(z) \cdot (\mathcal{T}(\epsilon_r^c)\boldsymbol{E}_0(z))$ and $\nabla \times \boldsymbol{w}(z) \cdot (\mathcal{T}(\mu_r)\boldsymbol{H}_0(z))$ as the object size, α, tends to zero where $(\boldsymbol{E}_0, \boldsymbol{H}_0)$ denote the solutions in the absence of the inclusion and $\boldsymbol{w}$ denotes a solution to the free space vector wave equation. Here, $\mu_r - 1 = \mu_*/\mu_0 - 1$ denotes the relative permeability perturbation, $\epsilon_r^c - 1 = 1/\epsilon_0(\epsilon_* - \mathrm{i}\sigma_*/\omega) - 1$ the complex permittivity perturbation and $\mathcal{T}(c)$ the rank 2 Pólya & Szegö (1951) polarization tensor parameterized by a contrast c. This tensor contains information about the shape and material properties of the inclusion, simplifies to a multiple of the identity tensor for a sphere and is diagonalizable for an ellipsoid (Ammari & Kang, 2007). Although the perturbation in complex permittivity does include the possibility of describing a conducting object in a non-conducting background this result is only applicable to wave propagation (electromagnetic scattering) problems at fixed wavenumber $k := \omega\sqrt{\epsilon_0\mu_0}$, where ϵ_0, μ_0 denote the free space values of permittivity and permeability, respectively.

Asymptopic formulae that describe the perturbation in the electromagnetic fields in unbounded domains due to the presence of a conducting dielectric (and/or magnetic) inclusion have also been obtained for the situation where $\alpha \to 0$ (for fixed k) (Ammari & Volkov, 2005; Ledger & Lionheart, 2015) and also for a non-conducting dielectric (magnetic) object where $k \to 0$ (for fixed α) (Baum, 1971; Dassios & Kleinman, 2000; Keller *et al.*, 1972; Kleinman, 1967, 1973; Kleinman & Senior, 1982; Ledger & Lionheart, 2015). The leading order terms in these results can also be expressed in terms of the rank 2 (Pólya & Szegö, 1951) polarization tensor parameterized by μ_r and ϵ_r^c (μ_r and $\epsilon_r := \epsilon_*/\epsilon_0$ for the latter). The former category applies when the inclusion is small and conducting, but not to the low-frequency case of $k \to 0$, while the latter does apply when $k \to 0$, but only for a non-conducting

object. Hence neither category describes the situation in magnetic induction where the inclusion is conducting and the frequency is small.

Ammari *et al.* (2014b) have recently obtained an asymptotic expansion, which, for the first time, correctly describes the perturbed magnetic field as $\alpha \to 0$ for a conducting (possibly magnetic and multiply connected) object in the presence of a low-frequency background magnetic field, generated by a coil with an alternating current. Rather than consider the limit as $k \to 0$ for the full time-harmonic Maxwell system, they instead consider the eddy current model where the displacement currents are neglected. The leading order term they obtain is written in terms of two new polarization tensors, called the permeability and conductivity tensors, which have different ranks, and the background magnetic field evaluated at the position of the centre of the inclusion. An algorithm for identifying conducting objects from induction data based on a process of classification by matching against a library of precomputed polarization tensors has also recently been proposed by Ammari *et al.* (2014a).

Our new contributions include considering, in detail, the properties of the conductivity and permeability tensors introduced by Ammari *et al.* (2014b). These studies enable us to show that, in practice, each of the tensors can be represented by just nine components in an orthonormal coordinate frame. We show that it is also possible to express the perturbed magnetic field in terms of a reduced rank 2 conductivity tensor and introduce a new symmetric rank 2 tensor, different from the Pólya & Szegö (1951) tensor, which describes the inclusion in terms of just six independent components. For a simple object, with rotational or mirror symmetries, we show that the number of independent coefficients is still fewer. These results have important consequences for characterizing conducting objects of different shapes and, in particular, target identification using dictionary based inverse algorithms. We include a description of an efficient numerical approach for accurately computing these new tensors, which is based on the regularized eddy current formulation using *hp*-finite elements presented in Ledger & Zaglmayr (2010). We also present simulations, which indicate an excellent agreement between the asymptotic formula of Ammari *et al.* using the numerically computed polarization tensors and the fields obtained from solving the full eddy current problem, for a range of case studies.

The presentation of the paper proceeds as follows: in Section 2, we describe the mathematical model and simplifying assumptions made about the problem under consideration. Then, in Section 3, we quote the asymptotic formula of Ammari *et al.* (2014b) and choose to express it in an alternative form containing a single rank 4 tensor. In this section, we also state our main result, which shows that their asymptotic formula can instead be written in terms of a new symmetric rank 2 polarization tensor, then, in Section 4, we prove a series of lemmas required for the proof of our main result. In Section 5, we discuss how further reductions in the number of independent components can be obtained if the object is rotationally symmetric or has mirror symmetries and the additional simplifications for a sphere. Then, in Section 6, we describe how the independent components of the tensors can be recovered from practical measurement data. In Section 7, we describe an approach to the numerical computation of the polarization tensors based on *hp*-finite elements, in Section 8, we present a series of numerical results to validate this approach and finish with our concluding remarks in 9.

2. Mathematical model

We follow Ammari *et al.* (2014b) and consider an electromagnetic inclusion in $\mathbb{R}^3$ of the form $B_\alpha = z + \alpha B$, where $B \subset \mathbb{R}^3$ is a bounded, smooth domain containing the origin. Let Γ and Γ_α denote the boundary of B and B_α, respectively, and μ_0 the permeability of free space. We continue to follow

their notation and write

$$\mu_\alpha = \begin{cases} \mu_* & \text{in } B_\alpha \\ \mu_0 & \text{in } \mathbb{R}^3 \setminus B_\alpha \end{cases} \qquad \sigma_\alpha = \begin{cases} \sigma_* & \text{in } B_\alpha \\ 0 & \text{in } \mathbb{R}^3 \setminus B_\alpha \end{cases}, \tag{2.1}$$

where μ_* and σ_* denote the object's permeability and conductivity, respectively, which we assume to be constant.

The time harmonic fields $\boldsymbol{E}_\alpha$ and $\boldsymbol{H}_\alpha$ that result from a time varying current source, $\boldsymbol{J}_0$, located a positive distance from B_α and satisfying $\nabla \cdot \boldsymbol{J}_0 = 0$ in $\mathbb{R}^3$, and their interaction with the object B_α, satisfy the eddy current equations (Ammari *et al.*, 2000)

$$\nabla \times \boldsymbol{E}_\alpha = \mathrm{i}\omega\mu_\alpha \boldsymbol{H}_\alpha \quad \text{in } \mathbb{R}^3, \tag{2.2a}$$

$$\nabla \times \boldsymbol{H}_\alpha = \sigma_\alpha \boldsymbol{E}_\alpha + \boldsymbol{J}_0 \quad \text{in } \mathbb{R}^3, \tag{2.2b}$$

$$\boldsymbol{E}_\alpha(\boldsymbol{x}) = O(|\boldsymbol{x}|^{-1}),\ \boldsymbol{H}_\alpha(\boldsymbol{x}) = O(|\boldsymbol{x}|^{-1}) \quad \text{as } |\boldsymbol{x}| \to \infty, \tag{2.2c}$$

where ω denotes the angular frequency. Letting $\alpha = 0$ in (2.2) we obtain the corresponding fields, $\boldsymbol{E}_0$ and $\boldsymbol{H}_0$, that result from time varying current source in the absence of an object. As described by Ammari *et al.* (2000) and Hiptmair (2002), the eddy current model is completed by $\nabla \cdot \boldsymbol{E}_\alpha = 0$ in B_α^c. Furthermore, Ammari *et al.* (2000) show that uniqueness of $\boldsymbol{E}_\alpha$ in B_α^c is achieved by additionally specifying

$$\int_{\Gamma_\alpha} \hat{\boldsymbol{n}} \cdot \boldsymbol{E}_\alpha \Big|_+ \mathrm{d}\boldsymbol{x} = 0, \tag{2.3}$$

and that, in practice, the decay of the fields is actually faster than the $|\boldsymbol{x}|^{-1}$ stated in the original eddy current model.

The task is to describe the leading order term for the perturbation $\boldsymbol{H}_\alpha(\boldsymbol{x}) - \boldsymbol{H}_0(\boldsymbol{x})$, caused by the presence of the object B_α, in terms of a polarization tensor, which is independent of position, with all positional dependence appearing only through the evaluation of background fields.

3. Main result

For the eddy current model described above, Theorem 3.2 in Ammari *et al.* (2014b) describes the perturbed magnetic field at positions $\boldsymbol{x}$ away from $\boldsymbol{z}$, due to the presence of object B_α, as $\alpha \to 0$ when $\nu := \alpha^2\omega\mu_0\sigma_* = O(1)$, such that ω grows asymptotically as fast as $1/\alpha^2$, which we choose to write in the alternative form stated below:[1]

THEOREM 3.1 Let $\nu = O(1)$ and $\alpha \to 0$ then, for $\boldsymbol{x}$ away from the location of the inclusion $\boldsymbol{z}$,

$$(\boldsymbol{H}_\alpha - \boldsymbol{H}_0)(\boldsymbol{x})_j = (\boldsymbol{D}_{\boldsymbol{x}}^2 G(\boldsymbol{x},\boldsymbol{z}))_{\ell m} \mathcal{M}_{\ell m j i} (\boldsymbol{H}_0(\boldsymbol{z}))_i + (\boldsymbol{R}(\boldsymbol{x}))_j, \tag{3.1}$$

where $G(\boldsymbol{x},\boldsymbol{z}) = 1/4\pi\,|\boldsymbol{x}-\boldsymbol{z}|$ is the free space Laplace Green's function, $|\boldsymbol{R}(\boldsymbol{x})| \leqslant C\alpha^4 \|\boldsymbol{H}_0\|_{W^{2,\infty}(B_\alpha)}$ such that $\boldsymbol{R}(\boldsymbol{x}) = O(\alpha^4)$ is a small remainder term and C is as defined in Ammari *et al.* (2014b). In the above,

[1] Note that I_3 on p. 10 of Ammari *et al.* (2014b) requires that $\nabla_{\boldsymbol{x}} G(\boldsymbol{x}, \alpha\boldsymbol{\xi} + \boldsymbol{z})) - \nabla_{\boldsymbol{x}} G(\boldsymbol{x},\boldsymbol{z}) - \alpha \boldsymbol{D}_{\boldsymbol{x}}^2 G(\boldsymbol{x},\boldsymbol{z})\boldsymbol{\xi} = O(\alpha^2)$, but instead the correct choice is $\nabla_{\boldsymbol{x}} G(\boldsymbol{x}, \alpha\boldsymbol{\xi} + \boldsymbol{z})) - \nabla_{\boldsymbol{x}} G(\boldsymbol{x},\boldsymbol{z}) + \alpha \boldsymbol{D}_{\boldsymbol{x}}^2 G(\boldsymbol{x},\boldsymbol{z})\boldsymbol{\xi} = O(\alpha^2)$, which adds a minus sign to the definition of $\mathcal{P}$ in (3.2).

Einstein summation convention is used,

$$\mathcal{M}_{\ell mji} := \mathcal{P}_{\ell mji} + \hat{\hat{\mathcal{N}}}_{\ell mji}, \quad \hat{\hat{\mathcal{N}}}_{kmji} := \delta_{kj}\delta_{m\ell}\mathcal{N}_{\ell i},$$

are components of rank 4 tensors in an orthonormal coordinate system and

$$\mathcal{P}_{\ell mji} := -\frac{\mathrm{i}\nu\alpha^3}{2}\hat{\boldsymbol{e}}_j \cdot \left(\hat{\boldsymbol{e}}_\ell \times \int_B \xi_m(\boldsymbol{\theta}_i + \hat{\boldsymbol{e}}_i \times \boldsymbol{\xi})\,\mathrm{d}\boldsymbol{\xi}\right), \tag{3.2}$$

$$\mathcal{N}_{\ell i} := \alpha^3\left(1 - \frac{\mu_0}{\mu_*}\right)\int_B \left(\hat{\boldsymbol{e}}_\ell \cdot \hat{\boldsymbol{e}}_i + \frac{1}{2}\hat{\boldsymbol{e}}_\ell \cdot \nabla \times \boldsymbol{\theta}_i\right)\mathrm{d}\boldsymbol{\xi}. \tag{3.3}$$

Furthermore, $\hat{\boldsymbol{e}}_i$ is a unit vector for the ith Cartesian coordinate direction, $(\boldsymbol{\xi})_m = \xi_m$ is the mth component of $\boldsymbol{\xi}$[2] and $\boldsymbol{\theta}_i$, $i = 1, 2, 3$, are the solutions to the transmission problem

$$\nabla_{\boldsymbol{\xi}} \times \mu^{-1}\nabla_{\boldsymbol{\xi}} \times \boldsymbol{\theta}_i - \mathrm{i}\omega\sigma\alpha^2\boldsymbol{\theta}_i = \mathrm{i}\omega\sigma\alpha^2\hat{\boldsymbol{e}}_i \times \boldsymbol{\xi} \quad \text{in } B \cup B^c, \tag{3.4a}$$

$$\nabla_{\boldsymbol{\xi}} \cdot \boldsymbol{\theta}_i = 0 \quad \text{in } B^c, \tag{3.4b}$$

$$[\boldsymbol{\theta}_i \times \hat{\boldsymbol{n}}]_\Gamma = \boldsymbol{0}, \quad [\mu^{-1}\nabla_{\boldsymbol{\xi}} \times \boldsymbol{\theta}_i \times \hat{\boldsymbol{n}}]_\Gamma = -2[\mu^{-1}]_\Gamma\hat{\boldsymbol{e}}_i \times \hat{\boldsymbol{n}} \quad \text{on } \Gamma, \tag{3.4c}$$

$$\boldsymbol{\theta}_i(\boldsymbol{\xi}) = O(|\boldsymbol{\xi}|^{-1}) \quad \text{as } |\boldsymbol{\xi}| \to \infty, \tag{3.4d}$$

where $\boldsymbol{\xi}$ is measured from the centre of B. By additionally specifying an analogues condition to (2.3) the uniqueness of $\boldsymbol{\theta}_i$ in B^c can be achieved.

Proof. Considering Theorem 3.2 in Ammari *et al.* (2014b), rewriting it in tensoral notation and then extending $\mathcal{N} = \mathcal{N}_{ji}\hat{\boldsymbol{e}}_j \otimes \hat{\boldsymbol{e}}_i$ to $\hat{\hat{\mathcal{N}}} = \hat{\hat{\mathcal{N}}}_{\ell mji}\hat{\boldsymbol{e}}_\ell \otimes \hat{\boldsymbol{e}}_m \otimes \hat{\boldsymbol{e}}_j \otimes \hat{\boldsymbol{e}}_i$ the result (3.1) immediately follows. However, it remains to show that $\mathcal{P} = \mathcal{P}_{\ell mji}\hat{\boldsymbol{e}}_\ell \otimes \hat{\boldsymbol{e}}_m \otimes \hat{\boldsymbol{e}}_j \otimes \hat{\boldsymbol{e}}_i$ and $\mathcal{N}$ are indeed rank 4 and rank 2 tensors in an orthonormal coordinate frame, respectively. To do so it suffices to show that their components obey appropriate transformation rules. In Proposition 4.3 in Ammari *et al.* (2014a) an equivalent statement to

$$\mathcal{P}'_{\ell mki} = \mathcal{R}_{\ell r}\mathcal{R}_{ms}\mathcal{R}_{kt}\mathcal{R}_{iu}\mathcal{P}_{rstu}, \tag{3.5}$$

for an orthogonal rotation $\mathcal{R}$ with determinate $|\mathcal{R}| = 1$ is shown. Repeating similar steps to the proof of Proposition 4.3 in Ammari *et al.* (2014a), but now tracking $|\mathcal{R}|$, we see that (3.5) also holds for the case where $\mathcal{R} = \mathcal{R}_{ji}\hat{\boldsymbol{e}}_j \otimes \hat{\boldsymbol{e}}_i$ is orthogonal with $|\mathcal{R}| = \pm 1$ and hence the components of $\mathcal{P}$ transform as a rank 4 tensor. Introducing $\tilde{\mu}_r = \mu_r = \mu_*/\mu_0$ in B and $\tilde{\mu}_r = 1$ in B^c then, by writing the components of $\mathcal{N}$ in the alternative equivalent form

$$\mathcal{N}_{ji} = \alpha^3[\tilde{\mu}_r^{-1}]_\Gamma\left(\int_B \hat{\boldsymbol{e}}_i \cdot \hat{\boldsymbol{e}}_j\,\mathrm{d}\boldsymbol{\xi} + \frac{1}{2}\int_\Gamma \hat{\boldsymbol{e}}_j \times \hat{\boldsymbol{n}}^- \cdot \boldsymbol{\theta}_i\Big|_-\,\mathrm{d}\boldsymbol{\xi}\right),$$

[2] We will use the notation ξ_m for the mth component of $\boldsymbol{\xi}$, but retain the notation $(\boldsymbol{H}_0(z))_i$ in (3.1) for the ith element of $\boldsymbol{H}_0(z)$ to ensure consistency with Ammari *et al.* (2014b).

following similar steps and using a notation similar to that in Proposition 4.3 in Ammari *et al.* (2014a) we obtain for $|\mathcal{R}| = \pm 1$ that

$$\begin{aligned}
\mathcal{N}_{ji}[\mathcal{R}(B)] &= \alpha^3[\tilde{\mu}_r^{-1}]_{\partial(\mathcal{R}(B))}\left(\int_{\mathcal{R}(B)}\delta_{ij}\,\mathrm{d}\boldsymbol{\xi} + \frac{1}{2}\int_{\partial\mathcal{R}(B)}\hat{\boldsymbol{e}}_j\times\hat{\boldsymbol{n}}(\boldsymbol{\xi})\cdot\boldsymbol{F}_{\mathcal{R}(B),\hat{\boldsymbol{e}}_i}(\boldsymbol{\xi})\,\mathrm{d}\boldsymbol{\xi}\right)\\
&= \alpha^3[\tilde{\mu}_r^{-1}]_\Gamma\left(\int_B\delta_{ij}\,\mathrm{d}\boldsymbol{\xi} + \frac{1}{2}\int_\Gamma\hat{\boldsymbol{e}}_j\times(\mathcal{R}\hat{\boldsymbol{n}}(\boldsymbol{\xi}))\cdot(|\mathcal{R}|\mathcal{R}\boldsymbol{F}_{B,\mathcal{R}^T\hat{\boldsymbol{e}}_i}(\boldsymbol{\xi}))\,\mathrm{d}\boldsymbol{\xi}\right)\\
&= \alpha^3[\tilde{\mu}_r^{-1}]_\Gamma\left(\int_B\mathcal{R}_{ip}\mathcal{R}_{jq}\delta_{pq}\,\mathrm{d}\boldsymbol{\xi} + \frac{|\mathcal{R}|^2}{2}\int_\Gamma(\mathcal{R}((\mathcal{R}^T\hat{\boldsymbol{e}}_j)\times\hat{\boldsymbol{n}}(\boldsymbol{\xi})))\cdot(\mathcal{R}\boldsymbol{F}_{B,\mathcal{R}^T\hat{\boldsymbol{e}}_i}(\boldsymbol{\xi}))\,\mathrm{d}\boldsymbol{\xi}\right)\\
&= \alpha^3[\tilde{\mu}_r^{-1}]_\Gamma\left(\int_B\mathcal{R}_{ip}\mathcal{R}_{jq}\delta_{pq}\,\mathrm{d}\boldsymbol{\xi} + \frac{1}{2}\int_\Gamma(\mathcal{R}^T\hat{\boldsymbol{e}}_j)\times\hat{\boldsymbol{n}}(\boldsymbol{\xi})\cdot\boldsymbol{F}_{B,\mathcal{R}^T\hat{\boldsymbol{e}}_i}(\boldsymbol{\xi})\,\mathrm{d}\boldsymbol{\xi}\right)\\
&= \alpha^3[\tilde{\mu}_r^{-1}]_\Gamma\mathcal{R}_{ip}\mathcal{R}_{jq}\left(\int_B\delta_{pq}\,\mathrm{d}\boldsymbol{\xi} + \frac{1}{2}\int_\Gamma\hat{\boldsymbol{e}}_q\times\hat{\boldsymbol{n}}(\boldsymbol{\xi})\cdot\boldsymbol{F}_{B,\hat{\boldsymbol{e}}_p}(\boldsymbol{\xi})\,\mathrm{d}\boldsymbol{\xi}\right)\\
&= \mathcal{R}_{ip}\mathcal{R}_{jq}\mathcal{N}_{pq}[B],
\end{aligned}$$

where δ_{pq} is the Kronecker delta, $\boldsymbol{F}_{\mathcal{R}(B),\hat{\boldsymbol{e}}_i}(\mathcal{R}\boldsymbol{\xi}) = |\mathcal{R}|\mathcal{R}\boldsymbol{F}_{B,\mathcal{R}^T\hat{\boldsymbol{e}}_i}(\boldsymbol{\xi})$ has been applied in the first step and $\boldsymbol{F}_{B,\mathcal{R}^T\hat{\boldsymbol{e}}_i} = \sum_{p=1}^3\mathcal{R}_{ip}\boldsymbol{F}_{B,\hat{\boldsymbol{e}}_p}$ has been applied in the second to last step. Note that the former follows from Proposition 4.3 in Ammari *et al.* (2014a), but without assuming that $|\mathcal{R}| = 1$, and the latter also follows from the same proposition. Thus, in abbreviated notation, it follows that

$$\mathcal{N}'_{ji} = \mathcal{R}_{jp}\mathcal{R}_{iq}\mathcal{N}_{pq},$$

so that the components of $\mathcal{N}$ transform as a rank 2 tensor. It immediately follows that $\widehat{\widehat{\mathcal{N}}}$ and $\mathcal{M}$ are rank 4 tensors. Note that in this theorem, and throughout the remainder, we use the notation of a hat to denote the extension of a tensor to a higher rank and a check to denote its corresponding contraction. □

REMARK 3.1 Note that in (3.1) the jth component of the perturbed field is an index of the rank 4 tensor $\mathcal{M} = \mathcal{M}_{\ell mji}\hat{\boldsymbol{e}}_\ell\otimes\hat{\boldsymbol{e}}_m\otimes\hat{\boldsymbol{e}}_j\otimes\hat{\boldsymbol{e}}_i$ and that $\boldsymbol{D}_{\boldsymbol{x}}^2G(\boldsymbol{x},\boldsymbol{z}) = (\boldsymbol{D}_{\boldsymbol{x}}^2G(\boldsymbol{x},\boldsymbol{z}))_{\ell m}\hat{\boldsymbol{e}}_\ell\otimes\hat{\boldsymbol{e}}_m$ appears as a double contraction with $\mathcal{M}$ with summation over ℓ and m. This is in contrast to other related results for perturbed electromagnetic fields. For instance, in Ammari *et al.* (2001) the perturbed magnetic field for small conducting object for the full Maxwell system is described in terms of the rank 2 Pólya & Szegö (1951) polarization tensor, which only appears as a single contraction with the background field solution. We address this apparent contradiction in the following theorem, which is our main result.

THEOREM 3.2 Let $\nu = O(1)$ and $\alpha\to 0$ then, for $\boldsymbol{x}$ away from the location of the inclusion $\boldsymbol{z}$,

$$(\boldsymbol{H}_\alpha - \boldsymbol{H}_0)(\boldsymbol{x})_j = (\boldsymbol{D}_{\boldsymbol{x}}^2G(\boldsymbol{x},\boldsymbol{z}))_{jm}\widetilde{\widetilde{\mathcal{M}}}_{mi}(\boldsymbol{H}_0(\boldsymbol{z}))_i + (\boldsymbol{R}(\boldsymbol{x}))_j, \tag{3.6}$$

where $\widetilde{\widetilde{\mathcal{M}}}_{mi} := -\check{\mathcal{C}}_{mi} + \mathcal{N}_{mi}$ are the components of the symmetric rank 2 tensor $\widetilde{\widetilde{\mathcal{M}}}$ in an orthonormal coordinate frame. Furthermore, $\mathcal{N}_{mi}$ is defined in (3.3),

$$\check{\mathcal{C}}_{mi} := -\frac{\mathrm{i}\nu\alpha^3}{4}\hat{\boldsymbol{e}}_m\cdot\int_B\boldsymbol{\xi}\times(\boldsymbol{\theta}_i + \hat{\boldsymbol{e}}_i\times\boldsymbol{\xi})\,\mathrm{d}\boldsymbol{\xi}. \tag{3.7}$$

and $\boldsymbol{\theta}_i$, $i = 1,2,3$, are the solutions to the transmission problem (3.4).

Proof. The proof immediately follows from Lemmas 4.3 and 4.4 stated in Section 4 where Lemma 4.3 establishes that $(\boldsymbol{D}_{\boldsymbol{x}}^2 G(\boldsymbol{x},\boldsymbol{z}))_{\ell m}\mathcal{M}_{\ell mji} = (\boldsymbol{D}_{\boldsymbol{x}}^2 G(\boldsymbol{x},\boldsymbol{z}))_{jm}\overgtr{\mathcal{M}}_{mi}$ and Lemma 4.4 establishes that $\overgtr{\mathcal{M}}$ is complex symmetric. □

REMARK 3.2 Evaluating (3.6) in the direction $\hat{\boldsymbol{q}}$ at location $\boldsymbol{s}$ we obtain

$$\hat{\boldsymbol{q}} \cdot (\boldsymbol{H}_\alpha - \boldsymbol{H}_0)(\boldsymbol{s}) = \tilde{\boldsymbol{H}}_0(\boldsymbol{z}) \cdot (\overgtr{\mathcal{M}}\boldsymbol{H}_0(\boldsymbol{z})) + \Delta, \tag{3.8}$$

where, in particular, we have choosen $\boldsymbol{H}_0(\boldsymbol{z}) := \boldsymbol{D}_{\boldsymbol{x}}^2 G(\boldsymbol{t},\boldsymbol{z})\hat{\boldsymbol{m}}$ as the (idealized) background magnetic field generated by a coil at position $\boldsymbol{t}$ with dipole moment $\hat{\boldsymbol{m}}$, set $\tilde{\boldsymbol{H}}_0(\boldsymbol{z}) := \boldsymbol{D}_{\boldsymbol{x}}^2 G(\boldsymbol{s},\boldsymbol{z})\hat{\boldsymbol{q}}$, as the background magnetic field that would be generated by a coil at position $\boldsymbol{s}$ with dipole moment $\hat{\boldsymbol{q}}$, and $\Delta := \hat{\boldsymbol{q}} \cdot \boldsymbol{R}(\boldsymbol{x})$. Written in this form, (3.8) agrees with the prediction in the engineering literature, e.g. Baum (1971), Das *et al.* (1990), Marsh *et al.* (2013) and Norton & Won (2001), which postulate that the magnetic field perturbation can be described in terms of a complex symmetric rank 2 polarization tensor. However, to the best of our knowledge, this is the first time that a rigorous mathematical justification and explicit formula is now available for the six components of the complex symmetric rank 2 tensor $\overgtr{\mathcal{M}}$ in an orthonormal coordinate frame.

REMARK 3.3 If the object is non-conducting and magnetic so that $\sigma_* = 0$ and $\mu_* \neq \mu_0$, then, provided that B_α is a simply connected smooth object, the tensor $\mathcal{N}$ reduces to a symmetric polarization tensor parameterized by a contrast $\mu_r := \mu_*/\mu_0$ in the object (Ammari *et al.*, 2014b). This, in turn, also agrees with the first order generalized polarization tensor of Ammari & Kang (2007) and the Pólya & Szegö (1951) polarization tensor whose (real) components in an orthonormal coordinate frame are

$$(\mathcal{N})_{ij} = \mathcal{T}(\mu_r)_{ij} = \alpha^3(\mu_r - 1)|B|\delta_{ij} + \alpha^3(\mu_r - 1)^2 \int_\Gamma \hat{\boldsymbol{n}} \cdot \nabla\phi_i \xi_j \, \mathrm{d}\boldsymbol{\xi}, \tag{3.9}$$

where ϕ_i, $i = 1, 2, 3$, satisfies the transmission problem

$$\nabla^2\phi_i = 0 \quad \text{in } B \cup B^c, \tag{3.10a}$$

$$[\phi_i]_\Gamma = 0, \quad \frac{\partial\phi_i}{\partial\hat{\boldsymbol{n}}}\bigg|_+ - \mu_r \frac{\partial\phi_i}{\partial\hat{\boldsymbol{n}}}\bigg|_- = \frac{\partial\xi_i}{\partial\hat{\boldsymbol{n}}} \quad \text{on } \Gamma, \tag{3.10b}$$

$$\phi_i \to 0 \quad \text{as } |\boldsymbol{\xi}| \to \infty. \tag{3.10c}$$

4. Proof of lemmas for the main result

We prove a number of lemmas that will be useful for the proof of our main result. Throughout the following the components of the tensors are taken to be with respect to an orthonormal (although not necessarily right handed) coordinate frame.

LEMMA 4.1 The components of the conductivity tensor $\mathcal{P}$ can be expressed as

$$\mathcal{P}_{\ell mji} = \varepsilon_{j\ell s}\breve{\mathcal{P}}_{msi} = \varepsilon_{j\ell s}\mathcal{C}_{msi}, \tag{4.1}$$

where ε is the alternating tensor with components

$$\varepsilon_{ijk} := \begin{cases} 1 & ijk \text{ even permutation of } 123 \\ -1 & ijk \text{ odd permutation of } 123 \\ 0 & \text{otherwise} \end{cases},$$

and $\mathcal{C}$ is rank 3 tensor density. The components of $\mathcal{C}$ are

$$\mathcal{C}_{msi} := \beta \int_B \xi_m(\theta_{si} + \varepsilon_{spq}\delta_{pi}\xi_q)\,\mathrm{d}\boldsymbol{\xi} = -\frac{\mathrm{i}\nu\alpha^3}{2}\hat{\boldsymbol{e}}_s \cdot \int_B \xi_m(\boldsymbol{\theta}_i + \hat{\boldsymbol{e}}_i \times \boldsymbol{\xi})\,\mathrm{d}\boldsymbol{\xi},$$

where $\beta := -\mathrm{i}\nu\alpha^3/2$.

Proof. It suffices to write the components of $\mathcal{P}$ in the alternative form

$$\begin{aligned} \mathcal{P}_{\ell mji} &= \beta\delta_{tj}\varepsilon_{t\ell s}\int_B \xi_m(\theta_{si} + \varepsilon_{spq}\delta_{pi}\xi_q)\,\mathrm{d}\boldsymbol{\xi} = \beta\varepsilon_{j\ell s}\int_B \xi_m(\theta_{si} + \varepsilon_{siq}\xi_q)\,\mathrm{d}\boldsymbol{\xi} \\ &= \varepsilon_{j\ell s}\breve{\mathcal{P}}_{msi} = \varepsilon_{j\ell s}\mathcal{C}_{msi}, \end{aligned} \tag{4.2}$$

where θ_{si} are the coefficents of the rank 2 tensor whose columns are $\boldsymbol{\theta}_i$. Furthermore, $\mathcal{C}$ is a rank 3 tensor density with components $\mathcal{C}_{msi} = \breve{\mathcal{P}}_{msi} = \frac{1}{2}\varepsilon_{sj\ell}\mathcal{P}_{\ell mji}$. □

Corollary 4.1 It follows from Lemma 4.1 that

$$\mathcal{P}_{\ell mji} = \varepsilon_{j\ell s}\mathcal{C}_{msi} = -\varepsilon_{\ell js}\mathcal{C}_{msi} = -\mathcal{P}_{jm\ell i},$$

which means that $\mathcal{P}_{\ell mji}$ is skew-symmetric with respect to the indices ℓ and j.

Lemma 4.2 The rank 3 tensor density $\mathcal{C}$ is skew symmetric with respect to the first two indices.

Proof. Starting from

$$\boldsymbol{e}_i \times \boldsymbol{\xi} = -\boldsymbol{\theta}_i + \frac{\mu_0}{\mathrm{i}\nu}\nabla \times \mu_*^{-1}\nabla \times \boldsymbol{\theta}_i, \tag{4.3}$$

in B where the subscript $\boldsymbol{\xi}$ on ∇ has been dropped (here and subsequently) for simplicity of notation, it follows by application of the alternating tensor that

$$\xi_m = \frac{1}{2}\varepsilon_{kpm}\hat{\boldsymbol{e}}_k \cdot \left(-\boldsymbol{\theta}_p + \frac{\mu_0}{\mathrm{i}\nu}\nabla \times \mu_*^{-1}\nabla \times \boldsymbol{\theta}_p\right), \tag{4.4}$$

in B. It is useful to define $\chi_m := \frac{1}{2}\varepsilon_{kpm}\hat{\boldsymbol{e}}_k \cdot (-\boldsymbol{\theta}_p + (1/\mathrm{i}\nu)\nabla \times \tilde{\mu}_r^{-1}\nabla \times \boldsymbol{\theta}_p)$ where $\tilde{\mu}_r := \mu/\mu_0$ such that $\tilde{\mu}_r = \mu_r = \mu_*/\mu_0$ in B and $\tilde{\mu}_r = 1$ in B^c. Note also that $\nabla \times \nabla \times \boldsymbol{\theta}_i = \boldsymbol{0}$ in B^c so that $\chi_m = -\frac{1}{2}\varepsilon_{kpm}\hat{\boldsymbol{e}}_k \cdot \boldsymbol{\theta}_p$

in B^c. Taking this into consideration then we can write

$$\begin{aligned}\mathcal{C}_{msi} &= \beta \int_B \chi_m \nabla \chi_s \cdot (\boldsymbol{\theta}_i + \hat{\boldsymbol{e}}_i \times \boldsymbol{\xi})\, \mathrm{d}\boldsymbol{\xi} \\ &= -\frac{\alpha^3}{2}\left(\int_B \nabla \times (\hat{\boldsymbol{e}}_s \xi_m) \cdot \tilde{\mu}_r^{-1} \nabla \times \boldsymbol{\theta}_i \, \mathrm{d}\boldsymbol{\xi} + \int_B \nabla \cdot (\tilde{\mu}_r^{-1} \nabla \times \boldsymbol{\theta}_i \times \chi_m \nabla \chi_s)\, \mathrm{d}\boldsymbol{\xi}\right) \\ &= -\frac{\alpha^3}{2}\left(\int_B \hat{\boldsymbol{e}}_m \times \hat{\boldsymbol{e}}_s \cdot \tilde{\mu}_r^{-1} \nabla \times \boldsymbol{\theta}_i \, \mathrm{d}\boldsymbol{\xi} - \int_\Gamma \chi_m \nabla \chi_s \cdot \tilde{\mu}_r^{-1} (\nabla \times \boldsymbol{\theta}_i \times \hat{\boldsymbol{n}}^-)\Big|_- \mathrm{d}\boldsymbol{\xi}\right).\end{aligned}$$

By using the transmission conditions in (3.4), $[\chi_m \nabla \chi_s \times \hat{\boldsymbol{n}}]_\Gamma = \mathbf{0}$ and the fact that the integrand in the last integral can alternatively be written in terms of a tangential trace and a twisted tangential trace, we obtain

$$\begin{aligned}\int_\Gamma \chi_m \nabla \chi_s \cdot (\tilde{\mu}_r^{-1} \nabla \times \boldsymbol{\theta}_i \times \hat{\boldsymbol{n}}^-)\Big|_- \mathrm{d}\boldsymbol{\xi} &= -\int_\Gamma \chi_m \nabla \chi_s \cdot \nabla \times \boldsymbol{\theta}_i \times \hat{\boldsymbol{n}}^+\Big|_+ \mathrm{d}\boldsymbol{\xi} \\ &\quad + 2[\tilde{\mu}_r^{-1}]_\Gamma \int_\Gamma \chi_m \nabla \chi_s \cdot \hat{\boldsymbol{e}}_i \times \hat{\boldsymbol{n}}^-\, \mathrm{d}\boldsymbol{\xi}. \qquad (4.5)\end{aligned}$$

First consider,

$$\begin{aligned}2[\tilde{\mu}_r^{-1}]_\Gamma \int_\Gamma \chi_m \nabla \chi_s \cdot \hat{\boldsymbol{e}}_i \times \hat{\boldsymbol{n}}^-\, \mathrm{d}\boldsymbol{\xi} &= 2[\tilde{\mu}_r^{-1}]_\Gamma \int_B \nabla \cdot (\chi_m \nabla \chi_s \times \hat{\boldsymbol{e}}_i)\, \mathrm{d}\boldsymbol{\xi} \\ &= 2[\tilde{\mu}_r^{-1}]_\Gamma \varepsilon_{ksi} \int_B \nabla \xi_m \cdot \nabla \xi_k \, \mathrm{d}\boldsymbol{\xi} = 2[\tilde{\mu}_r^{-1}]_\Gamma |B| \varepsilon_{msi}, \qquad (4.6)\end{aligned}$$

by the properties of χ_m in B. Secondly, noting that $\boldsymbol{\theta}_p = O(|\boldsymbol{\xi}|^{-2})$ and $\nabla \times \boldsymbol{\theta}_p = O(|\boldsymbol{\xi}|^{-3})$ as $|\boldsymbol{\xi}| \to \infty$ (Ammari *et al.*, 2014b) it follows that $\chi_m = O(|\boldsymbol{\xi}|^{-2})$ and $\nabla \chi_m = O(|\boldsymbol{\xi}|^{-3})$ (since $\boldsymbol{\theta}_p$ solves a Laplace equation with appropriate decay conditions in an unbounded domain exterior to a sufficiently large sphere that encloses B in a similar way to Proposition 3.1 in Ammari *et al.*, 2000). Then, we can apply integration by parts to

$$\begin{aligned}&\int_{B^c} \chi_m \nabla \chi_s \cdot \nabla \times \nabla \times \boldsymbol{\theta}_i \, \mathrm{d}\boldsymbol{\xi} = 0 \\ &= \int_{B^c} \nabla \chi_m \times \nabla \chi_s \cdot \nabla \times \boldsymbol{\theta}_i \, \mathrm{d}\boldsymbol{\xi} - \int_\Gamma \chi_m \nabla \chi_s \cdot \nabla \times \boldsymbol{\theta}_i \times \hat{\boldsymbol{n}}^+\Big|_+ \mathrm{d}\boldsymbol{\xi}, \qquad (4.7)\end{aligned}$$

where the aforementioned decay conditions imply that the far field integral drops out. By rearrangement and inserting (4.7) and (4.6) into (4.5) we have

$$\int_\Gamma \chi_m \nabla \chi_s \cdot (\nabla \times \boldsymbol{\theta}_i \times \hat{\boldsymbol{n}}^-)\Big|_- \mathrm{d}\boldsymbol{\xi} = -\int_{B^c} \nabla \chi_m \times \nabla \chi_s \cdot \nabla \times \boldsymbol{\theta}_i \, \mathrm{d}\boldsymbol{\xi} + 2[\tilde{\mu}_r^{-1}]_\Gamma |B| \varepsilon_{msi},$$

so that

$$\mathcal{C}_{msi} = -\frac{\alpha^3}{2}\left(\int_B \hat{\boldsymbol{e}}_m \times \hat{\boldsymbol{e}}_s \cdot \mu_r^{-1} \nabla \times \boldsymbol{\theta}_i \, \mathrm{d}\boldsymbol{\xi} + \int_{B^c} \nabla \chi_m \times \nabla \chi_s \cdot \nabla \times \boldsymbol{\theta}_i \, \mathrm{d}\boldsymbol{\xi} - 2[\tilde{\mu}_r^{-1}]_\Gamma |B| \varepsilon_{msi}\right).$$

Thus $\mathcal{C}_{msi} = -\mathcal{C}_{smi}$ as required. □

COROLLARY 4.2 The skew symmetry of $\mathcal{C}$ proved in Lemma 4.2 implies the tensor density has only nine independent components. It immediately follows that a rank 2 tensor $\breve{\mathcal{C}} = \breve{\breve{\mathcal{P}}}$ with components

$$\begin{aligned}\breve{\breve{\mathcal{P}}}_{ni} &:= \frac{1}{2}\varepsilon_{nms}\breve{\mathcal{P}}_{msi} = \frac{1}{4}\varepsilon_{nms}\varepsilon_{sjl}\mathcal{P}_{\ell mji} = \frac{1}{2}\varepsilon_{nms}\mathcal{C}_{msi} \\ &= \frac{\beta}{2}\hat{\boldsymbol{e}}_n \cdot \int_B \boldsymbol{\xi} \times (\boldsymbol{\theta}_i + \hat{\boldsymbol{e}}_i \times \boldsymbol{\xi}) \mathrm{d}\boldsymbol{\xi} =: \breve{\mathcal{C}}_{ni}, \end{aligned} \tag{4.8}$$

can be introduced such that $\mathcal{C}_{msi} = \varepsilon_{msk}\breve{\mathcal{C}}_{ki}$.

LEMMA 4.3 The components of double contraction between $\boldsymbol{D}_{\boldsymbol{x}}^2 G(\boldsymbol{x}, \boldsymbol{z})$ and $\mathcal{M}$ can be expressed as

$$(\boldsymbol{D}_{\boldsymbol{x}}^2 G(\boldsymbol{x}, \boldsymbol{z}))_{\ell m}\mathcal{M}_{\ell mji} = (\boldsymbol{D}_{\boldsymbol{x}}^2 G(\boldsymbol{x}, \boldsymbol{z}))_{jk}\breve{\breve{\mathcal{M}}}_{ki}, \tag{4.9}$$

where $\breve{\breve{\mathcal{M}}}$ is a rank 2 tensor with components $\breve{\breve{\mathcal{M}}}_{ki} := -\breve{\mathcal{C}}_{ki} + \mathcal{N}_{ki}$.

Proof. By writing

$$(\boldsymbol{D}_{\boldsymbol{x}}^2 G(\boldsymbol{x}, \boldsymbol{z}))_{\ell m} = \frac{1}{4\pi r^3}(3(\hat{\boldsymbol{r}} \otimes \hat{\boldsymbol{r}})_{\ell m} - \delta_{lm}) = \frac{1}{4\pi r^3}(3\hat{r}_\ell \hat{r}_m - \delta_{lm}),$$

where $\boldsymbol{r} = \boldsymbol{x} - \boldsymbol{z}$, $r = |\boldsymbol{r}|$ and $\hat{\boldsymbol{r}} = \boldsymbol{r}/r$, it is clear that $\boldsymbol{D}_{\boldsymbol{x}}^2 G(\boldsymbol{x}, \boldsymbol{z})$ has the properties

$$(\boldsymbol{D}_{\boldsymbol{x}}^2 G(\boldsymbol{x}, \boldsymbol{z}))_{\ell m} = (\boldsymbol{D}_{\boldsymbol{x}}^2 G(\boldsymbol{x}, \boldsymbol{z}))_{m\ell}, \quad \mathrm{tr}(\boldsymbol{D}_{\boldsymbol{x}}^2 G(\boldsymbol{x}, \boldsymbol{z})) = (\boldsymbol{D}_{\boldsymbol{x}}^2 G(\boldsymbol{x}, \boldsymbol{z}))_{\ell\ell} = 0.$$

Using this in combination with Lemma 4.1, Corollary 4.2 and the definition of $\mathcal{M}_{\ell mji}$ the result immediately follows. □

A consequence of Lemma 4.3 is that the components $\mathcal{P}_{\ell mji}$ and $\widehat{\widehat{\mathcal{N}}}_{\ell mji}$ of $\mathcal{M}_{\ell mji}$ form the disjoint skew-symmetric and symmetric parts of the total tensor with respect to indices ℓ and j, respectively.

LEMMA 4.4 The tensor $\breve{\mathcal{C}}$ is complex symmetric if $\mu_* = \mu_0$ and the tensor $\breve{\breve{\mathcal{M}}} = -\breve{\mathcal{C}} + \mathcal{N}$ is complex symmetric for a general conducting magnetic object.

Proof. The proof builds on a result stated in a preprint of Ammari *et al.* (2014b). We begin by rewriting the components of $\breve{\mathcal{C}}$ in an alternative form, to do so we consider

$$\int_B \boldsymbol{\xi} \times (\boldsymbol{\theta}_i + \hat{\boldsymbol{e}}_i \times \boldsymbol{\xi})\, \mathrm{d}\boldsymbol{\xi} \cdot \hat{\boldsymbol{e}}_j = \int_B (\boldsymbol{\theta}_i + \hat{\boldsymbol{e}}_i \times \boldsymbol{\xi}) \cdot \hat{\boldsymbol{e}}_j \times \boldsymbol{\xi}\, \mathrm{d}\boldsymbol{\xi}, \tag{4.10}$$

by properties of the scalar triple product. Thus, by using (3.4),

$$\begin{aligned}\int_B (\boldsymbol{\theta}_i + \hat{\boldsymbol{e}}_i \times \boldsymbol{\xi}) \cdot \hat{\boldsymbol{e}}_j \times \boldsymbol{\xi}\, \mathrm{d}\boldsymbol{\xi} &= \frac{\mu_0}{\mathrm{i}\nu\mu_*}\int_B \nabla \times \nabla \times \boldsymbol{\theta}_i \cdot \hat{\boldsymbol{e}}_j \times \boldsymbol{\xi}\, \mathrm{d}\boldsymbol{\xi} \\ &= \frac{1}{\mathrm{i}\nu}\int_B \frac{1}{\tilde{\mu}_r}\nabla \times \nabla \times \boldsymbol{\theta}_i \cdot \left(\frac{1}{\mathrm{i}\nu\tilde{\mu}_r}\nabla \times \nabla \times \boldsymbol{\theta}_j - \boldsymbol{\theta}_j\right) \mathrm{d}\boldsymbol{\xi}, \end{aligned} \tag{4.11}$$

where $\tilde{\mu}_r$ is as defined in Lemma 4.2. Performing integration by parts

$$\int_B \frac{1}{\tilde{\mu}_r}\nabla\times\nabla\times\boldsymbol{\theta}_i\cdot\boldsymbol{\theta}_j\,\mathrm{d}\boldsymbol{\xi} = \int_B \frac{1}{\tilde{\mu}_r}\nabla\times\boldsymbol{\theta}_j\cdot\nabla\times\boldsymbol{\theta}_i\,\mathrm{d}\boldsymbol{\xi} - \int_\Gamma \boldsymbol{\theta}_j\cdot\frac{1}{\tilde{\mu}_r}\nabla\times\boldsymbol{\theta}_i\times\hat{\boldsymbol{n}}^-\Big|_-\,\mathrm{d}\xi. \tag{4.12}$$

Next, using the transmission conditions on Γ in (3.4), then

$$\begin{aligned}\int_B(\boldsymbol{\theta}_i+\hat{\boldsymbol{e}}_i\times\boldsymbol{\xi})\cdot\hat{\boldsymbol{e}}_j\times\boldsymbol{\xi}\,\mathrm{d}\boldsymbol{\xi} &= \frac{1}{(\mathrm{i}\nu)^2}\int_B\frac{1}{\tilde{\mu}_r^2}\nabla\times\nabla\times\boldsymbol{\theta}_i\cdot\nabla\times\nabla\times\boldsymbol{\theta}_j\,\mathrm{d}\boldsymbol{\xi}\\ &\quad-\frac{1}{\mathrm{i}\nu}\int_B\frac{1}{\tilde{\mu}_r}\nabla\times\boldsymbol{\theta}_i\cdot\nabla\times\boldsymbol{\theta}_j\,\mathrm{d}\boldsymbol{\xi}+\frac{1}{\mathrm{i}\nu}\int_\Gamma\boldsymbol{\theta}_j\cdot\nabla\times\boldsymbol{\theta}_i\times\hat{\boldsymbol{n}}^-\Big|_+\,\mathrm{d}\boldsymbol{\xi}\\ &\quad+\frac{2[\tilde{\mu}_r^{-1}]_\Gamma}{\mathrm{i}\nu}\int_\Gamma\hat{\boldsymbol{e}}_i\times\hat{\boldsymbol{n}}^-\cdot\boldsymbol{\theta}_j\,\mathrm{d}\boldsymbol{\xi}.\end{aligned} \tag{4.13}$$

Then, by performing integration by parts in B^c,

$$\int_{B^c}\boldsymbol{\theta}_j\cdot\nabla\times\nabla\times\boldsymbol{\theta}_i\mathrm{d}\boldsymbol{\xi} = \int_{B^c}\nabla\times\boldsymbol{\theta}_i\cdot\nabla\times\boldsymbol{\theta}_j+\int_\Gamma\boldsymbol{\theta}_j\cdot\nabla\times\boldsymbol{\theta}_i\times\hat{\boldsymbol{n}}^-\Big|_+\,\mathrm{d}\boldsymbol{\xi}=0, \tag{4.14}$$

which is valid given the decay conditions on $\boldsymbol{\theta}_i$ and $\nabla\times\boldsymbol{\theta}_i$ as $|\boldsymbol{\xi}|\to\infty$ (Ammari *et al.*, 2014b). Using (4.14) in (4.13) and recalling (4.8) and (4.10), then we have that the components

$$\begin{aligned}\check{\mathcal{C}}_{ji} &= -\frac{\alpha^3}{4\mathrm{i}\nu}\int_B\frac{1}{\tilde{\mu}_r^2}\nabla\times\nabla\times\boldsymbol{\theta}_i\cdot\nabla\times\nabla\times\boldsymbol{\theta}_j\,\mathrm{d}\boldsymbol{\xi}\\ &\quad+\frac{\alpha^3}{4}\int_{B\cup B^c}\frac{1}{\tilde{\mu}_r}\nabla\times\boldsymbol{\theta}_i\cdot\nabla\times\boldsymbol{\theta}_j\,\mathrm{d}\boldsymbol{\xi}-\frac{\alpha^3[\tilde{\mu}_r^{-1}]_\Gamma}{2}\int_\Gamma\hat{\boldsymbol{e}}_i\times\hat{\boldsymbol{n}}^-\cdot\boldsymbol{\theta}_j\Big|_-\,\mathrm{d}\boldsymbol{\xi},\end{aligned}$$

are symmetric when $\mu_*=\mu_0$. We rewrite $\mathcal{N}_{ji}$ in the following form

$$\begin{aligned}\mathcal{N}_{ji} &= \alpha^3\left(1-\frac{\mu_0}{\mu_*}\right)\int_B\left(\hat{\boldsymbol{e}}_i+\frac{1}{2}\nabla\times\boldsymbol{\theta}_i\right)\mathrm{d}\boldsymbol{\xi}\cdot\hat{\boldsymbol{e}}_j\\ &= \alpha^3[\tilde{\mu}_r^{-1}]_\Gamma\left(\int_B\hat{\boldsymbol{e}}_i\cdot\hat{\boldsymbol{e}}_j\,\mathrm{d}\boldsymbol{\xi}+\frac{1}{2}\int_\Gamma\hat{\boldsymbol{e}}_j\times\hat{\boldsymbol{n}}^-\cdot\boldsymbol{\theta}_i\Big|_-\,\mathrm{d}\boldsymbol{\xi}\right).\end{aligned}$$

It then follows that the components of $\overset{\approx}{\mathcal{M}}=-\check{\mathcal{C}}+\mathcal{N}$ can be written as

$$\begin{aligned}\overset{\approx}{\mathcal{M}}_{ji} &= \frac{\alpha^3}{4\mathrm{i}\nu}\int_B\frac{1}{\tilde{\mu}_r^2}\nabla\times\nabla\times\boldsymbol{\theta}_i\cdot\nabla\times\nabla\times\boldsymbol{\theta}_j\,\mathrm{d}\boldsymbol{\xi}-\frac{\alpha^3}{4}\int_{B\cup B^c}\frac{1}{\tilde{\mu}_r}\nabla\times\boldsymbol{\theta}_i\cdot\nabla\times\boldsymbol{\theta}_j\,\mathrm{d}\boldsymbol{\xi}\\ &\quad+\alpha^3[\tilde{\mu}_r^{-1}]_\Gamma\left(\frac{1}{2}\int_\Gamma\hat{\boldsymbol{e}}_i\times\hat{\boldsymbol{n}}^-\cdot\boldsymbol{\theta}_j\Big|_-\,\mathrm{d}\boldsymbol{\xi}+\int_B\hat{\boldsymbol{e}}_i\cdot\hat{\boldsymbol{e}}_j\mathrm{d}\boldsymbol{\xi}+\frac{1}{2}\int_\Gamma\hat{\boldsymbol{e}}_j\times\hat{\boldsymbol{n}}^-\cdot\boldsymbol{\theta}_i\Big|_-\,\mathrm{d}\boldsymbol{\xi}\right),\end{aligned} \tag{4.15}$$

which are symmetric. □

5. Simplified polarization tensors for classes of geometries

The number of independent components that are required to define $\mathcal{C}$ and $\mathcal{N}$ (and hence $\check{\mathcal{C}}$, $\mathcal{P}$, $\hat{\hat{\mathcal{N}}}$, $\mathcal{M}$ and $\tilde{\tilde{\mathcal{M}}}$) in an orthonormal coordinate frame for an object with either a rotational or mirror symmetry (or multiple symmetries, or both) are often fewer than those required to define a general object. To explain this, we show how the number of independent components can be reduced for an object which has a uniaxial symmetry and an object which has mirror symmetries. We then apply similar techniques to a range of simple objects and consider the further simplification that results in the case of a spherical object.

5.1 *Polarization tensors for objects with uniaxial symmetry*

The number of independent components for an object, which has uniaxial symmetry, in a given direction, can either be determined by a counting argument or by considering the coefficents of the tensor that should remain invariant under a rotation. Here we apply the latter and first consider the conductivity tensor $\mathcal{P}$, which can be expressed in terms of the rank 3 tensor density $\mathcal{C}$. We remark that one could also express this in terms of the rank 2 tensor $\check{\mathcal{C}}$, but instead we apply the former and use the skew symmetry of $\mathcal{C}$. Under the transformation by an orthogonal matrix $\mathcal{R}$ the components of the rank 3 tensor density become

$$\mathcal{C}'_{ijk} = |\mathcal{R}|\mathcal{R}_{i\ell}\mathcal{R}_{jm}\mathcal{R}_{kn}\mathcal{C}_{\ell mn}, \tag{5.1}$$

where $|\mathcal{R}| = 1$ for a proper transformation. For example, for a rotation of angle ψ about $\hat{\boldsymbol{e}}_3$ then

$$\mathcal{R} = \begin{pmatrix} \cos\psi & \sin\psi & 0 \\ -\sin\psi & \cos\psi & 0 \\ 0 & 0 & 1 \end{pmatrix}.$$

If an object has uniaxial symmetry in the $\hat{\boldsymbol{e}}_3$ coordinate direction, then this means that the components of the tensor $\mathcal{C}$ should be invariant under a $\psi = \pi/2$ rotation about the $\hat{\boldsymbol{e}}_3$ axis : $\hat{\boldsymbol{e}}_1 \to \hat{\boldsymbol{e}}_2$ and $\hat{\boldsymbol{e}}_2 \to -\hat{\boldsymbol{e}}_1$. Under this transformation $\mathcal{C}' = \mathcal{C}$ and applying (5.1) to $\mathcal{C}'$ gives $\mathcal{C}'' = \mathcal{C}' = \mathcal{C}$. By considering a general $\mathcal{C}$ it follows that it is seven independent components are $\mathcal{C}_{333}$, $\mathcal{C}_{311} = \mathcal{C}_{322}$, $\mathcal{C}_{131} = \mathcal{C}_{232}$, $\mathcal{C}_{113} = \mathcal{C}_{223}$, $\mathcal{C}_{312} = -\mathcal{C}_{321}$, $\mathcal{C}_{132} = -\mathcal{C}_{231}$ and $\mathcal{C}_{123} = -\mathcal{C}_{213}$. But, we also know that $\mathcal{C}$ is skew symmetric with respect to the first two indices and this reduces the number to just 3: $\mathcal{C}_{312} = -\mathcal{C}_{321} = -\mathcal{C}_{132} = \mathcal{C}_{231}$, $\mathcal{C}_{123} = -\mathcal{C}_{213}$ and $\mathcal{C}_{311} = -\mathcal{C}_{131} = \mathcal{C}_{322} = -\mathcal{C}_{232}$.

Secondly, we consider the permeability tensor $\mathcal{N} = \mathcal{N}_{\ell i}\hat{\boldsymbol{e}}_\ell \otimes \hat{\boldsymbol{e}}_i$ which transforms as

$$\mathcal{N}'_{ij} = \mathcal{R}_{i\ell}\mathcal{R}_{jm}\mathcal{N}_{\ell m}. \tag{5.2}$$

Then, by proceeding in a similar manner to above, for an object with uniaxial symmetry in the $\hat{\boldsymbol{e}}_3$ direction we have $\mathcal{N}_{11} = \mathcal{N}_{22}$, $\mathcal{N}_{12} = -\mathcal{N}_{21}$ and $\mathcal{N}_{33}$.

Finally, we know that the total reduced tensor $\tilde{\tilde{\mathcal{M}}} = -\check{\mathcal{C}} + \mathcal{N}$ is symmetric, so that $\tilde{\tilde{\mathcal{M}}}_{12} = \tilde{\tilde{\mathcal{M}}}_{21}$, but rotational symmetry tell us $\mathcal{N}_{12} = -\mathcal{N}_{21}$ and $\check{\mathcal{C}}_{12} = -\check{\mathcal{C}}_{21} = \mathcal{C}_{232}$ so that $\tilde{\tilde{\mathcal{M}}}_{12} = \tilde{\tilde{\mathcal{M}}}_{21} = -\mathcal{C}_{232} + \mathcal{N}_{12} = \mathcal{C}_{232} - \mathcal{N}_{12} = 0$. Thus $\tilde{\tilde{\mathcal{M}}}$ is diagonal in this case with just two independent components: $\tilde{\tilde{\mathcal{M}}}_{11} = \tilde{\tilde{\mathcal{M}}}_{22} = \mathcal{N}_{11} - \mathcal{C}_{231}$ and $\tilde{\tilde{\mathcal{M}}}_{33} = \mathcal{N}_{33} - \mathcal{C}_{123}$.

5.2 *Polarization tensors for objects with both uniaxial and mirror symmetries*

The number of independent components that are required to define $\mathcal{C}$ and $\mathcal{N}$ can also be reduced if the object has mirror symmetries. For an object with a mirror symmetry associated with the plane with unit normal vector $\hat{\boldsymbol{n}}$ then

$$\mathcal{R}_{ij} = \delta_{ij} - 2\hat{n}_i\hat{n}_j. \tag{5.3}$$

The components of the rank 3 tensor density $\mathcal{C}$ and the rank 2 tensor $\mathcal{N}$ remain invariant under a reflection provided that the last index remains unchanged under the transformation. By following similar steps as outlined in Section 5.1 the independent components of $\mathcal{C}$ and $\mathcal{N}$ for objects with mirror symmetries can be obtained.

5.3 *Examples of symmetries in polarization tensors*

By applying similar arguments to those described above, the entries in Table 1, which lists the independent components for some simple shapes, can be identified. The rotational symmetries of an object about an angle π in a given coordinate direction, which are equivalent to an appropriate mirror symmetry, have been omitted. Note that the independent components that define a sphere and a cube are the same, as are the cases of a cylinder and a cone when their axes are aligned. Furthermore, for all the simple objects in Table 1, we observe that the rank 2 tensor $\overset{\approx}{\mathcal{M}} = -\check{\mathcal{C}} + \mathcal{N}$ is diagonal.

5.4 *Polarization tensor for a spherical geometry*

The polarization tensor for a spherical object, which has been obtained by Ammari *et al.* (2014b), is a further simplification of (3.6) with components $\overset{\approx}{\mathcal{M}}_{\ell i} = -\check{\mathcal{C}}_{\ell i} + \mathcal{N}_{\ell i} = (-C + N)\delta_{\ell i}$ such that $\overset{\approx}{\mathcal{M}}$ is a scalar multiple of the identity tensor. Here, it can be shown that

$$\begin{aligned} N &:= \frac{1}{3}\mathcal{N}_{pp}, \\ C &:= \frac{1}{6}\varepsilon_{msi}\mathcal{C}_{msi} = \frac{\beta}{6}\varepsilon_{msi}\int_B \xi_m(\theta_{si} + \varepsilon_{siq}\xi_q)\,\mathrm{d}\boldsymbol{\xi} \\ &= \frac{\beta}{6}\int_B (\varepsilon_{msi}\xi_m\theta_{si} + 2\xi_q\xi_q)\,\mathrm{d}\boldsymbol{\xi} = -\beta\int_B (\xi_1\boldsymbol{\theta}_2\cdot\boldsymbol{e}_3 - \xi_1^2)\,\mathrm{d}\boldsymbol{\xi}, \end{aligned}$$

by noting that $\int_B \xi_1^2\,\mathrm{d}\boldsymbol{\xi} = \int_B \xi_2^2\,\mathrm{d}\boldsymbol{\xi} = \int_B \xi_3^2\,\mathrm{d}\boldsymbol{\xi}$ for a sphere and using integration by parts to show that $\int_B \xi_1\boldsymbol{\theta}_3\cdot\boldsymbol{e}_2\,\mathrm{d}\boldsymbol{\xi} = -\int_B \xi_1\boldsymbol{\theta}_2\cdot\boldsymbol{e}_3\,\mathrm{d}\boldsymbol{\xi}$.

Using the analytical solution (Smythe, 1968) for the eddy currents generated in a conducting (magnetic) sphere of radius α with conductivity σ_*, permeability μ_* at angular frequency ω, when placed in a uniform field $\boldsymbol{H}_0$, we can show that the form of the perturbed field is identical to (3.6), if we set $\boldsymbol{R} = \boldsymbol{0}$ and $\overset{\approx}{\mathcal{M}}_{\ell i} = M\delta_{\ell i}$. It can also be identified that

$$\bar{M} = 2\pi\alpha^3\frac{((2\mu_* + \mu_0)\nu I_{-1/2} - (\mu_0(1+\nu^2) + 2\mu_*)I_{1/2})}{(\mu_* - \mu_0)I_{-1/2} + (\mu_0(1+\nu^2) - \mu_*)I_{1/2}}, \tag{5.4}$$

where $\nu = \sqrt{\mathrm{i}\sigma\mu_*\omega}\alpha$, $I_{1/2}(\nu) = \sqrt{2/\pi\nu}\sinh\nu$ and $I_{-1/2}(\nu) = \sqrt{2/\pi\nu}\cosh\nu$. The overline indicates the complex conjugate, which appears due to the $e^{\mathrm{i}\omega t}$ time variation in Smythe (1968) rather than the $\mathrm{e}^{-\mathrm{i}\omega t}$

TABLE 1 *Non-zero independent coefficients that are required to represent $\mathcal{C}$ and $\mathcal{N}$ for a range of simple objects*

Object shape	Rotational symmetries	Mirror symmetries	Independent coefficients in $\mathcal{C}$	Independent coefficients in $\mathcal{N}$
 Sphere	Isotropic	Infinite number of planes	$\mathcal{C}_{123} = -\mathcal{C}_{132} = -\mathcal{C}_{213} = \mathcal{C}_{231} = \mathcal{C}_{312} = -\mathcal{C}_{321}$	$\mathcal{N}_{11} = \mathcal{N}_{22} = \mathcal{N}_{33}$
 Cube: aligned with axes	Uniaxial about $\hat{\boldsymbol{e}}_1, \hat{\boldsymbol{e}}_2, \hat{\boldsymbol{e}}_3$	Planes with normals $\hat{\boldsymbol{e}}_1, \hat{\boldsymbol{e}}_2, \hat{\boldsymbol{e}}_3$, $(\hat{\boldsymbol{e}}_1 + \hat{\boldsymbol{e}}_2)/\sqrt{2}$, $(\hat{\boldsymbol{e}}_1 + \hat{\boldsymbol{e}}_3)/\sqrt{2}$, $(\hat{\boldsymbol{e}}_2 + \hat{\boldsymbol{e}}_3)/\sqrt{2}$	$\mathcal{C}_{123} = -\mathcal{C}_{132} = -\mathcal{C}_{213} = \mathcal{C}_{231} = \mathcal{C}_{312} = -\mathcal{C}_{321}$	$\mathcal{N}_{11} = \mathcal{N}_{22} = \mathcal{N}_{33}$
 Block: $\left(-\frac{w}{2}, -\frac{d}{2}, -\frac{h}{2}\right) \times \left(\frac{w}{2}, \frac{d}{2}, \frac{h}{2}\right)$ aligned with axes	None	Planes with normals $\hat{\boldsymbol{e}}_1, \hat{\boldsymbol{e}}_2, \hat{\boldsymbol{e}}_3$, $(d\hat{\boldsymbol{e}}_1 + w\hat{\boldsymbol{e}}_2)/\sqrt{d^2 + w^2}$ $(w\hat{\boldsymbol{e}}_3 + h\hat{\boldsymbol{e}}_1)/\sqrt{w^2 + h^2}$ $(h\hat{\boldsymbol{e}}_2 + d\hat{\boldsymbol{e}}_3)/\sqrt{d^2 + h^2}$	$\mathcal{C}_{123} = -\mathcal{C}_{213}$ $\mathcal{C}_{321} = -\mathcal{C}_{231}$ $\mathcal{C}_{132} = -\mathcal{C}_{312}$	$\mathcal{N}_{11}$ $\mathcal{N}_{22}$ $\mathcal{N}_{33}$
 Cone: axis aligned with $\hat{\boldsymbol{e}}_1$	Rotationally invariant about $\hat{\boldsymbol{e}}_1$	Planes with normals $\hat{\boldsymbol{e}}_2, \hat{\boldsymbol{e}}_3$ any plane $\perp$ base & passing through the vertex	$\mathcal{C}_{123} = -\mathcal{C}_{132} = -\mathcal{C}_{213} = \mathcal{C}_{312}$ $\mathcal{C}_{231} = -\mathcal{C}_{321}$	$\mathcal{N}_{11}$ $\mathcal{N}_{22} = \mathcal{N}_{33}$
 Cylinder: axis aligned with $\hat{\boldsymbol{e}}_1$	Rotationally invariant about $\hat{\boldsymbol{e}}_1$	Planes with normals $\hat{\boldsymbol{e}}_1, \hat{\boldsymbol{e}}_2, \hat{\boldsymbol{e}}_3$ any plane $\perp$ base & parallel to $\hat{\boldsymbol{e}}_1$	$\mathcal{C}_{123} = -\mathcal{C}_{132} = -\mathcal{C}_{213} = \mathcal{C}_{312}$ $\mathcal{C}_{231} = -\mathcal{C}_{321}$	$\mathcal{N}_{11}$ $\mathcal{N}_{22} = \mathcal{N}_{33}$
 Cube with hole: hole aligned with $\hat{\boldsymbol{e}}_3$	Uniaxial about $\hat{\boldsymbol{e}}_3$	Planes with normals $\hat{\boldsymbol{e}}_1, \hat{\boldsymbol{e}}_2, \hat{\boldsymbol{e}}_3$, $(\hat{\boldsymbol{e}}_1 + \hat{\boldsymbol{e}}_2)/\sqrt{2}$, $(\hat{\boldsymbol{e}}_1 + \hat{\boldsymbol{e}}_3)/\sqrt{2}$, $(\hat{\boldsymbol{e}}_2 + \hat{\boldsymbol{e}}_3)/\sqrt{2}$	$\mathcal{C}_{123} = -\mathcal{C}_{213}$ $\mathcal{C}_{132} = -\mathcal{C}_{231}$ $= \mathcal{C}_{321} = -\mathcal{C}_{312}$	$\mathcal{N}_{11} = \mathcal{N}_{22}$ $\mathcal{N}_{33}$
 Ellipsoid: general case	None	Planes with normals $\hat{\boldsymbol{e}}_1, \hat{\boldsymbol{e}}_2, \hat{\boldsymbol{e}}_3$	$\mathcal{C}_{123} = -\mathcal{C}_{213}$ $\mathcal{C}_{132} = -\mathcal{C}_{231}$ $\mathcal{C}_{321} = -\mathcal{C}_{312}$	$\mathcal{N}_{11}$ $\mathcal{N}_{22}$ $\mathcal{N}_{33}$

assumed here. Note that the asymptotic formula (3.6) implies that $|N - C - M| = O(\alpha^4)$ as $\alpha \to 0$ for fixed $\boldsymbol{x}$ and $\boldsymbol{z}$.

An analytical solution (Wait, 1953) is also available for case where the same sphere is now illuminated by an incident field generated by a circular coil of radius γ carrying an alternating current I. For a coil centred at $\boldsymbol{s}$ the incident magnetic field at position $\boldsymbol{z}$ can be described in terms of a magnetic dipole

in the form

$$\boldsymbol{H}_0(z) = \boldsymbol{D}_x^2 G(z,s)\boldsymbol{m}, \tag{5.5}$$

provided that the length of coil, $L = 2\pi\gamma$, is small compared with the distance from the coil to the object, $|z-s|$. In the above, $\boldsymbol{m}$ is the magnetic dipole moment of the current source, which, for a circular coil, has $|\boldsymbol{m}| = I\pi\gamma^2$ (Jackson, 1967). If the coil is chosen to lie in the $(\hat{\boldsymbol{e}}_1, \hat{\boldsymbol{e}}_2)$ plane, then $\boldsymbol{m} = I\pi\gamma^2\hat{\boldsymbol{e}}_3$ and

$$\boldsymbol{H}_0(z) = I\pi\gamma^2 \boldsymbol{D}_x^2 G(z,s)\hat{\boldsymbol{e}}_3. \tag{5.6}$$

Furthermore, we can show that the leading order term for $(\boldsymbol{H}_\alpha - \boldsymbol{H}_0)(\boldsymbol{x})$ that Wait (1953) obtains is identical to that described by (3.6).

6. Determining $\overset{\approx}{\mathcal{M}}$ from field measurements

In the next section, we describe a numerical approach for computing $\boldsymbol{\theta}_i$, $i = 1, 2, 3$, which can be used for the accurate calculation of the polarization tensors. However, there may also be situations (e.g. as part of an inverse algorithm or an experimental validation procedure) where the independent components that define the polarization tensors should be determined from field measurements of $(\boldsymbol{H}_\alpha - \boldsymbol{H}_0)(\boldsymbol{x})$. In particular, by taking sufficient measurements of $\hat{\boldsymbol{q}}^{(i)} \cdot (\boldsymbol{H}_\alpha - \boldsymbol{H}_0)(\boldsymbol{x}^{(i)})$ at different positions $\boldsymbol{x}^{(i)}$ and orientations $\hat{\boldsymbol{q}}^{(i)}$ an over-determined system can be built from which the six independent complex components of $\overset{\approx}{\mathcal{M}}$ in an orthonormal coordinate system can be found by solving this system in a least squares sense.

7. *hp*-Finite element methodology for the computation of $\overset{\approx}{\mathcal{M}}$

The computation of $\overset{\approx}{\mathcal{M}} = -\check{\mathcal{C}} + \mathcal{N}$ requires the approximate solution of the transmission problem (3.4), which in turn has similarities to the $\boldsymbol{A}$-based formulation of eddy current problems, e.g. Ledger & Zaglmayr (2010). We therefore advocate that the regularized formulation previously developed for eddy current problems on multiply connected domains be adapted for it is approximate solution. For this purpose, we truncate the otherwise unbounded domain B^c at a finite distance from the object and create the finite domain $\Omega = \tilde{B}^c \cup B$ and on the truncated boundary $\partial\Omega$ we impose $\nabla_\xi \times \boldsymbol{\theta}_i \times \hat{\boldsymbol{n}} = \boldsymbol{0}$.

7.1 *Regularized formulation*

Let $\boldsymbol{\vartheta}_i = \bar{\boldsymbol{\theta}}_i$. The transmission problem for $\boldsymbol{\vartheta}_i$ on the finite (computational) domain can then be written in the form

$$\begin{aligned}
&\nabla_\xi \times \tilde{\mu}_r^{-1} \nabla_\xi \times \boldsymbol{\vartheta}_i + \mathrm{i}\mu_0\omega\sigma\alpha^2\boldsymbol{\vartheta}_i = -\mathrm{i}\mu_0\omega\sigma\alpha^2\hat{\boldsymbol{e}}_i \times \boldsymbol{\xi} \quad \text{in } B \cup \tilde{B}^c,\\
&\nabla_\xi \cdot \boldsymbol{\vartheta}_i = 0 \quad \text{in } \tilde{B}^c,\\
&[\boldsymbol{\vartheta}_i \times \hat{\boldsymbol{n}}]_\Gamma = \boldsymbol{0}, \quad [\tilde{\mu}_r^{-1}\nabla_\xi \times \boldsymbol{\vartheta}_i \times \hat{\boldsymbol{n}}]_\Gamma = -2[\tilde{\mu}_r^{-1}]_\Gamma \hat{\boldsymbol{e}}_i \times \hat{\boldsymbol{n}} \quad \text{on } \Gamma,\\
&\nabla_\xi \times \boldsymbol{\vartheta}_i \times \hat{\boldsymbol{n}} = \boldsymbol{0} \quad \text{on } \partial\Omega,
\end{aligned}$$

where $\tilde{\mu}_r$ is as defined in Lemma 4.2.

Following Bachlinger *et al.* (2005, 2006), Ledger & Zaglmayr (2010), Zaglmayr (2006) and Zaglmayr & Schöberl (2005) we introduce the perturbed weak problem: Let $\tau > 0$ be a small perturbation parameter, then: find $\boldsymbol{\vartheta}_i^\tau \in \boldsymbol{H}(\mathrm{curl}, \Omega)$ such that

$$(\tilde{\mu}_r^{-1}\nabla_{\boldsymbol{\xi}} \times \boldsymbol{\vartheta}_i^\tau, \nabla_{\boldsymbol{\xi}} \times \boldsymbol{v})_\Omega + (\kappa \boldsymbol{\vartheta}_i^\tau, \boldsymbol{v})_\Omega = -(\kappa \hat{\boldsymbol{e}}_i \times \boldsymbol{\xi}, \boldsymbol{v})_B - 2\int_\Gamma [\tilde{\mu}_r^{-1}]\hat{\boldsymbol{e}}_i \times \hat{\boldsymbol{n}} \cdot \bar{\boldsymbol{v}}\, \mathrm{d}\boldsymbol{\xi}, \tag{7.1}$$

for all $\boldsymbol{v} \in \boldsymbol{H}(\mathrm{curl}, \Omega)$ where

$$\kappa = \begin{cases} \mathrm{i}\mu_0\omega\sigma_*\alpha^2 & \text{in } B \\ \tau & \text{in } \tilde{B}^c \end{cases}.$$

This regularized formulation circumvents the need to enforce the divergence constraint $\nabla_{\boldsymbol{\xi}} \cdot \boldsymbol{\vartheta}_i = 0$ in B^c (and an analogous integral condition to (2.3) on Γ) to enforce the uniqueness of $\boldsymbol{\theta}_i$ in B^c. Furthermore, the previous analysis of Bachlinger *et al.* (2005), Zaglmayr (2006), which considers the error associated with the solution of the perturbed eddy current problem, carries over to (7.1).

7.2 *Discrete approximation*

In this work we use the basis functions of Zaglmayr (2006) and Zaglmayr & Schöberl (2005) and we recall that for a tetrahedral triangulation consisting of vertices $\mathcal{V}_h$, edges $\mathcal{E}_h$, faces $\mathcal{F}_h$ and cells $\mathcal{T}_h$ their (reduced) hierarchic $\boldsymbol{H}(\mathrm{curl})$ and $H^1(\Omega)$ conforming finite element basis can be expressed in terms of the splitting

$$V_{h,p}^{\mathrm{red}} := V_h^{\mathcal{N}_0} \oplus \sum_{E\in\mathcal{E}_h^B} \nabla W_{p+1}^E \oplus \sum_{F\in\mathcal{F}_h^B} \nabla W_{p+1}^F \oplus \sum_{F\in\mathcal{F}_h} \tilde{V}_p^F \oplus \sum_{I\in\mathcal{T}_h^B} \nabla W_{p+1}^I \oplus \sum_{I\in\mathcal{T}_h} \tilde{V}_p^I,$$

and

$$W_{h,p+1} := W_{h,1} \oplus \sum_{E\in\mathcal{E}_h} W_{p+1}^E \oplus \sum_{F\in\mathcal{F}_h} W_{p+1}^F + \sum_{I\in\mathcal{T}_h} W_{p+1}^I \subset H^1(\Omega).$$

In the above $V_h^{\mathcal{N}_0}$ and $W_{h,1}$ denotes the set of lowest-order Nédélec (edge element) basis functions and the standard lowest order hat functions, respectively, the former being associated with the edges of the element and the latter with the vertices of the element. The extension to arbitrary high polynomial degree order consists of the enrichment of the finite element space through the addition of higher-order edge, face and interior-based basis functions, W_{p+1}^E, W_{p+1}^F and W_{p+1}^I, respectively, for H^1 and the addition of higher-order edge, face and interior functions for $\boldsymbol{H}(\mathrm{curl})$, where, in this case, the higher-order edge and some of the higher order face and interior functions are constructed from the gradients of their H^1 conforming counterparts. Furthermore, the superscript B on $\mathcal{E}_h$, $\mathcal{F}_h$ and $\mathcal{T}_h$ is used to denote those edges, faces and cells associated with subdomain B, only, as the gradient basis functions in $\tilde{B}^c$ are omitted. It then follows that the approximate weak formulation is: find $\boldsymbol{\vartheta}_{hp}^i \in V_{h,p}^{\mathrm{red}} \cap H(\mathrm{curl}, \Omega)$ such that

$$\begin{aligned}(\tilde{\mu}_r^{-1}\nabla_{\boldsymbol{\xi}} \times \boldsymbol{\vartheta}_{hp}^i, \nabla_{\boldsymbol{\xi}} \times \boldsymbol{v}_{hp})_\Omega + (\kappa \boldsymbol{\vartheta}_{hp}^i, \boldsymbol{v}_{hp})_\Omega \\ = -(\kappa \hat{\boldsymbol{e}}_i \times \boldsymbol{\xi}, \boldsymbol{v}_{hp})_B - 2\int_\Gamma [\tilde{\mu}_r^{-1}]\hat{\boldsymbol{e}}_i \times \hat{\boldsymbol{n}} \cdot \bar{\boldsymbol{v}}_{hp}\, \mathrm{d}\boldsymbol{\xi} \quad \forall \boldsymbol{v}_{hp} \in V_{h,p}^{\mathrm{red}} \cap H(\mathrm{curl}, \Omega).\end{aligned} \tag{7.2}$$

The structure of the left-hand side of (7.2) is analogous to the gauged $\boldsymbol{A}$-based formulation of eddy current problems and, therefore, the preconditioning technique described in Ledger & Zaglmayr (2010)

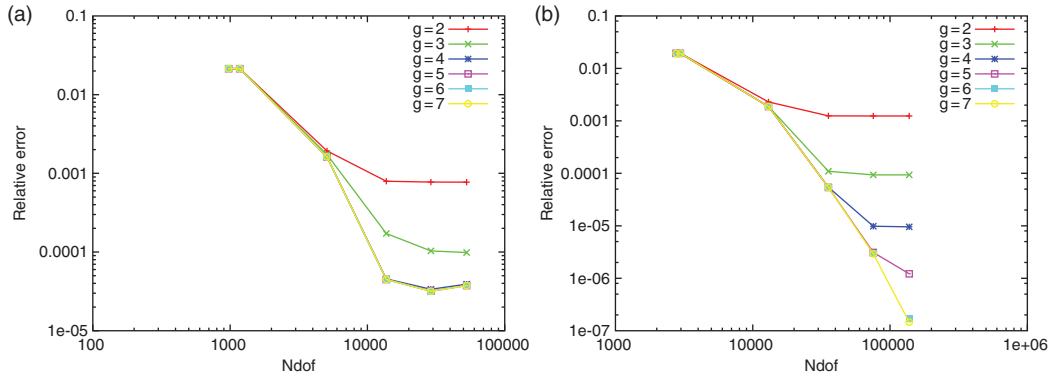

FIG. 1. Polarization tensor for a spherical object with $\alpha = 0.01$ m, $\sigma_* = 5.96 \times 10^7$ S m^{-1}, $\mu_* = \mu_0$ and 133.5 rad s^{-1} showing convergence of $\|\overleftrightarrow{\mathcal{M}} - \overleftrightarrow{\mathcal{M}}^{hp}\|_2 / \|\overleftrightarrow{\mathcal{M}}\|_2$ with $p = 0, 1, 2, 3, 4, 5$ and $g = 2, 3, 4, 5, 6, 7$ when (a) the domain is truncated at a radius of $10|B|$ and (b) the domain is truncated at a radius of $100|B|$.

can be immediately applied to the complex symmetric linear system that results ensuring a robust solver that is capable of coping with the large contrasts in κ.

For problems with curved geometry the approach described in Ledger & Coyle (2005) is employed, in which, for a degree of the polynomial correction, g, the coefficients of the edge and face corrections, $\boldsymbol{c}^E \in W^E_{g+1}$ and $\boldsymbol{c}^F \in W^F_{g+1}$, respectively, are determined by solving local L^2 minimization problems on the edges and faces of those elements lying on the curved boundary.

8. Numerical examples

8.1 *Polarization tensor for a spherical object*

For the case where B_α is a sphere of radius $\alpha = 0.01$ m, with $\sigma_* = 5.96 \times 10^7$ S m^{-1}, $\mu_* = \mu_0$ and $\omega = 133.5$ rad s^{-1}, so that $\nu = 1$, we present results, for the convergence of the error $\|\overleftrightarrow{\mathcal{M}} - \overleftrightarrow{\mathcal{M}}^{hp}\|_2 / \|\overleftrightarrow{\mathcal{M}}\|_2$ with increasing numbers of degrees of freedom (Ndof) in Fig. 1. Note that $\|\cdot\|_2$ denotes the entry-wise norm for a rank 2 tensor, $\|\overleftrightarrow{\mathcal{M}}\|_2 = (\sum_{\ell m} |\overleftrightarrow{\mathcal{M}}_{\ell m}|^2)^{1/2}$, and $\overleftrightarrow{\mathcal{M}}^{hp}$ is the approximate polarization tensor computed using $\boldsymbol{\vartheta}^i_{hp}$, $i = 1, 2, 3$. To compute the numerical tensor, we consider the unit sphere B and choose Ω to be a sphere which is 10, and then 100, times the radius of B. For these geometries we generate (coarse) meshes of 880 and 2425 unstructured tetrahedra, respectively, for discretizing the two cases. These and subsequent meshes were generated using the NETGEN mesh generator (Schöberl, 1997). In order to represent the curved geometry of the sphere polynomial representations using degrees $g = 2, 3, 4, 5, 6, 7$ are considered and finite elements of order $p = 0, 1, 2, 3, 4, 5$ are used to obtain the approximate solutions $\boldsymbol{\vartheta}^i_{hp}$, $i = 1, 2, 3$. In each case use a regularization parameter, τ, that is eight orders of magnitude smaller than $\omega\sigma_*\mu_0\alpha^2$.

In each case, the lines represent the different choices of g and the points on the line represent increasing p. The convergence behaviour resembles that previously described in Ledger & Coyle (2005). In Fig. 1(a) we observe that, for truncation at a radius of $10|B|$, the error associated with the geometry dominates for low g as indicated by stagnation of the convergence curves for $g = 2, 3, 4$ with increasing p. For $g = 2, 3, 4$, we see improvements in accuracy as g is increased since the resolution of the geometry is improved with each increment of g. However, for $g \geqslant 4$, no further reduction in error can be achieved

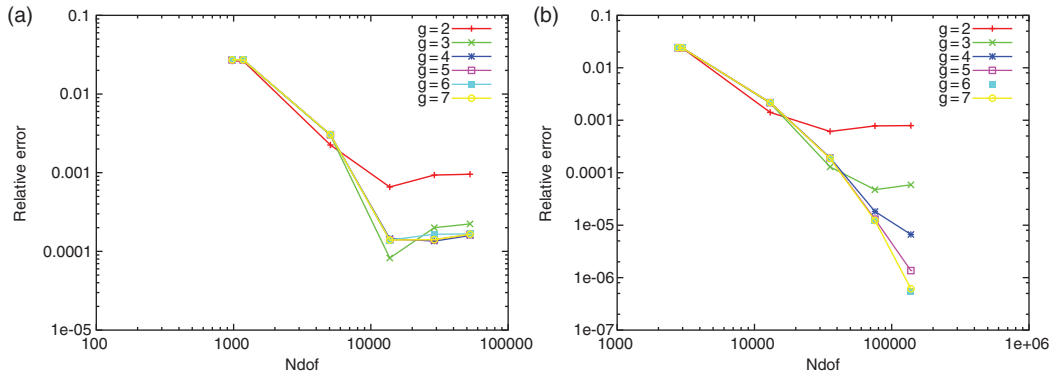

FIG. 2. Polarization tensor for a spherical object with $\alpha = 0.01$ m, $\sigma_* = 5.96 \times 10^7$ S m^{-1}, $\mu_* = 1.5\mu_0$ and 133.5 rad s^{-1} showing convergence of $\|\widetilde{\widetilde{\mathcal{M}}} - \widetilde{\widetilde{\mathcal{M}}}^{hp}\|_2 / \|\widetilde{\widetilde{\mathcal{M}}}\|_2$ with $p = 0, 1, 2, 3, 4, 5$ and $g = 2, 3, 4, 5, 6, 7$ when (a) the domain is truncated at a radius of $10|B|$ and (b) the domain is truncated at a radius of $100|B|$.

by increasing p alone, which means that the error associated with the artificial truncation of the boundary dominates over the error in resolving the curved boundary. On the other hand, by truncating at a radius of $100|B|$ and repeating the computations, as shown in Fig. 1(b), we now see that the boundary truncation error no longer dominates and, for $g \geqslant 6$, exponential convergence of the polarization tensor down to relative errors of 10^{-7} results by performing p-refinement.

The corresponding results for the same sized object with fictional parameters as before, except $\mu_* = 1.5\mu_0$, are shown in Fig. 2. For low g and truncation at either $10|B|$ or $100|B|$, the geometry error dominates but, for sufficiently high g and high p, the error can be reduced to $< 10^{-6}$ by truncating the domain at a radius of $100|B|$. In particular, for $g \geqslant 6$ and performing p-refinement, exponential convergence of the polarization tensor is achieved.

8.2 *Objects in a uniform background field*

For uniform $\boldsymbol{H}_0$ we compare $(\boldsymbol{H}_\alpha - \boldsymbol{H}_0)(\boldsymbol{x})$ predicted by (3.6), when hp-finite elements are used to numerically compute the rank 2 polarization tensor $\widetilde{\widetilde{\mathcal{M}}}^{hp}$, with the results obtained by solving the full eddy current problem, using hp-finite elements and the formulation in Ledger & Zaglmayr (2010). We undertake this comparison for a series of different shaped objects taken from Table 1 including when B_α is a sphere of radius 0.01 m, a 0.0075 m $\times$ 0.015 m $\times$ 0.01 m rectangular block, a cone with height 0.01 m and maximum radius 0.005 m and, finally, a cube of side length 0.01 m with a 0.005 m $\times$ 0.005 m $\times$ 0.01 m hole removed.

In each case, we select the far field boundary to be located at distance a 100 times the size of the object, for cases with curved geometries we use $g = 4$ and for approximating the solution to (7.2), we use $p = 4$ elements and meshes of 2425, 3433, 19,851 and 7377 unstructured tetrahedra for the cases of a sphere, block, cone and the cube with hole, respectively. We fix the material parameters as $\sigma_* = 5.96 \times 10^7$ S m^{-1}, $\mu_* = 1.5\mu_0$ and the angular frequency as 133.5 rad s^{-1} for all objects. The polarization tensor $\widetilde{\widetilde{\mathcal{M}}}^{hp}$ for each object is computed by considering an appropriate unit-sized object B, which, when an appropriate scaling is applied, results in the physical object B_α. Then, by assuming a uniform incident field $\boldsymbol{H}_0(\boldsymbol{x}) = \boldsymbol{H}_0 = \hat{\boldsymbol{e}}_3$ we compare $|(\boldsymbol{H}_\alpha - \boldsymbol{H}_0)(\boldsymbol{x})|/|\boldsymbol{H}_0(\boldsymbol{x})|$ when $\boldsymbol{x} = \boldsymbol{r} = r\hat{\boldsymbol{e}}_i \in B_\alpha^c$ and $r \leqslant 0.1$m and $i = 1, 2, 3$ in turn.

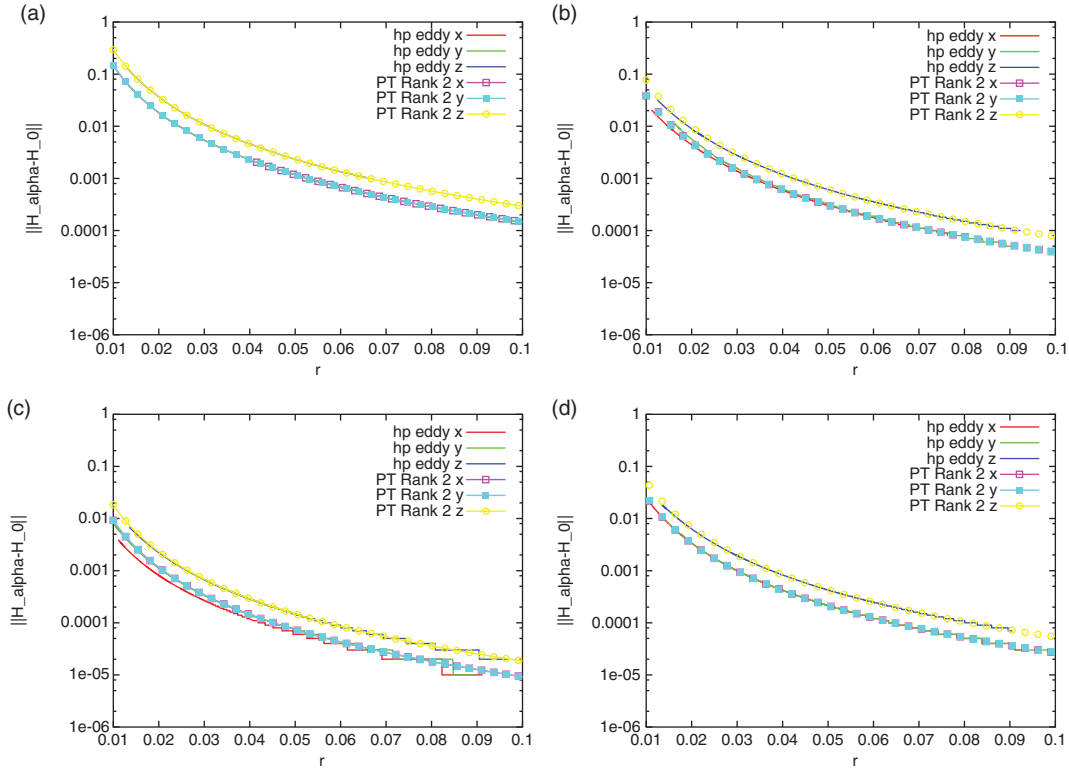

FIG. 3. Comparison of $|(\boldsymbol{H}_\alpha - \boldsymbol{H}_0)(\boldsymbol{x})|/|\boldsymbol{H}_0(\boldsymbol{x})|$ for uniform $\boldsymbol{H}_0(\boldsymbol{x}) = \boldsymbol{H}_0$ when $\boldsymbol{x} = \boldsymbol{r} = r\hat{\boldsymbol{e}}_i \in B_\alpha^c$ and $r \leqslant 0.1$ m for $i = 1, 2, 3$, in turn, showing the results obtained by using the numerically computed rank 2 polarization tensor $\overset{\approx}{\mathcal{M}}^{hp}$ and by solving the full eddy current problem when B_α is: (a) a sphere of radius 0.01 m, (b) a 0.0075 m × 0.015 m × 0.01 m rectangular block, (c) a cone with height 0.01 m and maximum radius 0.005 m and (d) a cube of side length 0.01 m with a 0.005 m × 0.005 m × 0.01 m hole removed.

The results of this investigation are shown in Fig. 3. For all cases, the perturbed field predicted by the numerically computed polarization tensor is in excellent agreement with that obtained by solving the full eddy current problem.

As a further illustration of the validity of the asymptotic formula (3.6) we compute $|(\boldsymbol{H}_\alpha - \boldsymbol{H}_0)(\boldsymbol{x}) - (\boldsymbol{D}_{\boldsymbol{x}}^2 G(\boldsymbol{x}, z)(\overset{\approx}{\mathcal{M}}^{hp}\boldsymbol{H}_0(z)))|/|\boldsymbol{H}_0(\boldsymbol{x})| = |\boldsymbol{R}(\boldsymbol{x})|/|\boldsymbol{H}_0(\boldsymbol{x})|$ for uniform $\boldsymbol{H}_0 = \hat{\boldsymbol{e}}_3$, fixed $\boldsymbol{x}, \boldsymbol{z}$ and varying α for the cases of a sphere and a spheroid with material parameters as in Fig. 3. We choose the radius of the sphere to be α and the minor and major axes of the spheroid to be α and 2α, respectively. For these objects, we numerically compute $\overset{\approx}{\mathcal{M}}^{hp}$ for $\alpha = 0.1, 0.075, 0.05, 0.025, 0.1$ m, in turn, using high fidelity discretizations consisting of uniform $p = 5, p = 7$ elements, geometry resolutions of $g = 7$ and $g = 4$ and meshes of 2742 and 15,493 unstructured tetrahedra for the cases of the sphere and spheroid, respectively, with truncation at $200|B|$ in both cases. For $\boldsymbol{H}_\alpha(\boldsymbol{x})$, we employ the aforementioned analytical solution for the sphere and a known result for a conducting permeable spheroid (Ao *et al.*, 2002). The results of this investigation are shown in Fig. 4, which confirm that $\boldsymbol{R}(\boldsymbol{x}) = O(\alpha^4)$ in the asymptotic formula (3.6). Note that in the case of the sphere $|\boldsymbol{R}(\boldsymbol{x})|$ is converging faster than α^4, which is consistent with the Landau notation.

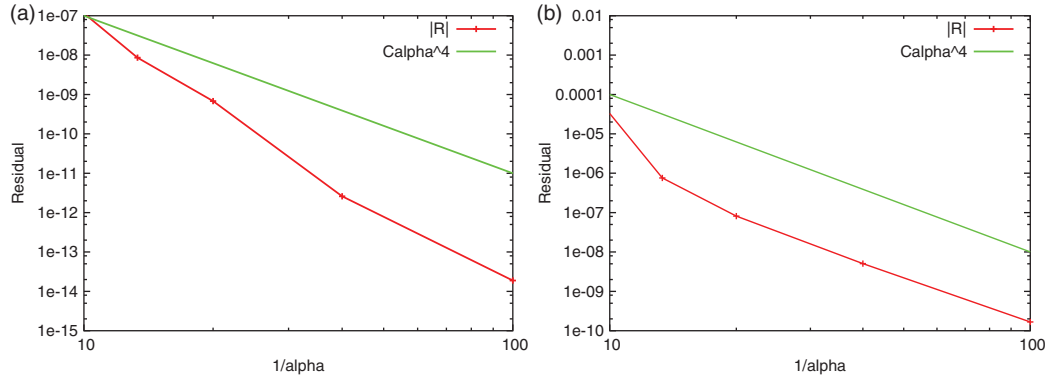

FIG. 4. Comparison of $|(\boldsymbol{H}_\alpha - \boldsymbol{H}_0)(\boldsymbol{x}) - (\boldsymbol{D}^2_{\boldsymbol{x}} G(\boldsymbol{x},\boldsymbol{z})(\widetilde{\widetilde{\mathcal{M}}}^{hp}\boldsymbol{H}_0(\boldsymbol{z})))|/|\boldsymbol{H}_0(\boldsymbol{x})| = |\boldsymbol{R}(\boldsymbol{x})|/|\boldsymbol{H}_0(\boldsymbol{x})|$ and $C\alpha^4$ for uniform $\boldsymbol{H}_0 = \hat{\boldsymbol{e}}_3$, fixed $\boldsymbol{x}$ and $\boldsymbol{z}$ with varying α for the cases of a (a) a conducting permeable sphere and (b) a conducting permeable spheroid where $\widetilde{\widetilde{\mathcal{M}}}^{hp}$ has been computed using high-fidelity discretizations.

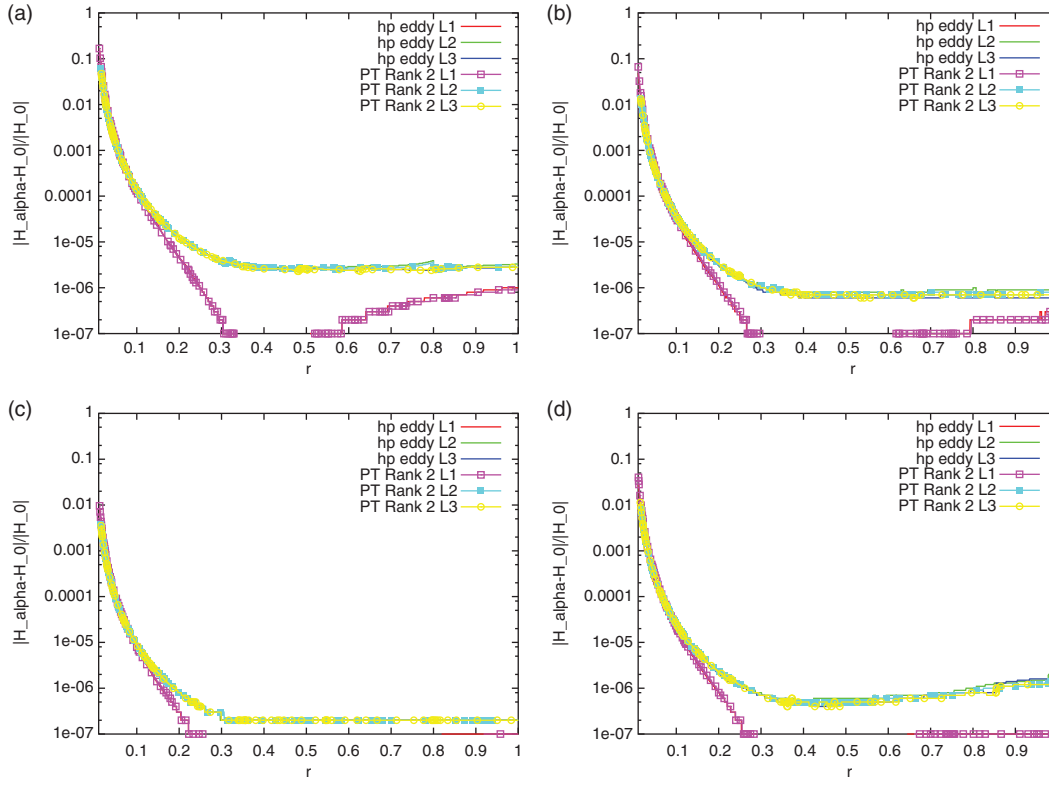

FIG. 5. Comparison of $|(\boldsymbol{H}_\alpha - \boldsymbol{H}_0)(\boldsymbol{x})|/|\boldsymbol{H}_0(\boldsymbol{x})|$ for rotational $\boldsymbol{H}_0$ along the lines L1, L2 and L3, in turn, showing the results obtained by using the numerically computed rank 2 polarization tensor $\widetilde{\widetilde{\mathcal{M}}}^{hp}$ and by solving the full eddy current problem when B_α is: (a) a sphere of radius 0.01 m, (b) a 0.0075 m × 0.015 m × 0.01 m rectangular block, (c) a cone with height 0.01 m and maximum radius 0.005 m and (d) a cube of side length 0.01 m with a 0.005 m × 0.005 m × 0.01 m hole removed.

8.3 *Objects in a rotational background field*

In this section, we perform a similar comparison with that undertaken in Section 8.2 but now with $\boldsymbol{H}_0(\boldsymbol{x})$ generated by a coil carrying a current such that $|\boldsymbol{J}_0| = 1 \times 10^6\,\mathrm{Am}^{-2}$. The coil is taken to be a torus of inner radius 0.005 m and outer radius 0.01 m and has position $0.4\hat{\mathbf{e}}_3$ m relative to the centre of the object. The shape and material properties of the different objects are as described in Section 8.2. We undertake comparisons of $|(\boldsymbol{H}_\alpha - \boldsymbol{H}_0)(\boldsymbol{x})|/|\boldsymbol{H}_0(\boldsymbol{x})|$ when $\boldsymbol{x} = \boldsymbol{r} = x_3\hat{\boldsymbol{e}}_3 \in B_\alpha^c$ (L1), $\boldsymbol{x} = \boldsymbol{r} = x_1\hat{\boldsymbol{e}}_1 + x_3\hat{\boldsymbol{e}}_3 \in B_\alpha^c$ (L2) and $\boldsymbol{x} = \boldsymbol{r} = x_2\hat{\boldsymbol{e}}_2 + x_3\hat{\boldsymbol{e}}_3 \in B_\alpha^c$ (L3) for $r = |\boldsymbol{x}| \leqslant 1$ m using $p = 4$ elements and $g = 4$ when the geometry is curved. The meshes for computing the solution to the full eddy current problem consist of 36,012, 35,347, 49,086 and 53,743 unstructured tetrahedra for the cases of a sphere, block, cone and the cube with hole, respectively, where the coil has also been discretized in each case.

The results of this investigation are shown in Fig. 5. In particular, we show how the normalized field changes with distance along a line directly above the object (L1) and along two diagonal lines extending upwards from the object (L2 and L3). For all objects considered, the agreement between the perturbed field predicted by the asymptotic expansion and (3.6) using the numerically computed $\overgtr{\mathcal{M}}^{hp}$ and those obtained by solving the full eddy current problem is excellent.

The small differences between the results predicted by (3.6) and solving the full eddy current problem for large r are attributed to the artificial truncation boundary used for solving the full eddy current problem, which, for these examples, has been placed at $r = 2$ m. These differences are not noticeable in Fig. 3 as the results are shown for small r, significantly further away from the artificial truncation boundary.

9. Conclusion

In this article, we have shown that the rank 4 conductivity tensor, $\mathcal{P}$, obtained by Ammari *et al.* (2014b) that appears in the leading order term for the perturbed magnetic field, in the presence of a conducting object at low frequencies as $\alpha \to 0$ when $\nu = 1$, can be expressed in terms of the rank 3 tensor density $\mathcal{C}$ and this in turn can be expressed in terms of rank 2 tensor $\check{\mathcal{C}}$. By using properties of these tensors, we have shown that at most nine independent components are required for defining $\check{\mathcal{C}}$ in an orthonormal coordinate frame, and hence $\mathcal{P}$, for a conducting object. A further nine are required for the rank 2 tensor $\mathcal{N}$ if the object is magnetic. Furthermore, we have shown that the perturbed field for a general object is influenced by a reduced rank 2 symmetric tensor $\overgtr{\mathcal{M}} := -\check{\mathcal{C}} + \mathcal{N}$ with just six complex independent components in an orthonormal coordinate frame. If the object has rotational or mirror symmetries we have shown that the number of independent components can be reduced further.

We have included results to illustrate how the tensors can be computed accurately by using the *hp*-finite element method. These results indicate that, for smooth objects, exponential convergence of the computed tensor can be achieved by performing *p*-refinement on a coarse grid with accurate geometry and a far field boundary placed sufficiently far from the object. We have also used these the *hp*-finite element approach to numerically verify the perturbed fields predicted by the asymptotic formula for a range of objects and illuminations and all show excellent agreement when compared with solving the full eddy current problem. In future work, we intend to develop an alternative coupled finite element boundary integral approach for solving the transmission problem (3.4), without the need to introduce the artificial regularization parameter τ in (7.1), and imposing a constraint of the form $\int_\Gamma \hat{\boldsymbol{n}} \cdot \boldsymbol{\theta}_i|_+ \,\mathrm{d}\boldsymbol{\xi} = 0$ (Hiptmair, 2002).

Acknowledgements

The authors are very grateful to Prof. H. Ammari, J. Chen and D. Volkov for their helpful discussions and comments and would also like to thank EPSRC for the financial support received from the grants EP/K00428X/1 and EP/K039865/1 and the support received from the land mine research charity Find A Better Way.

Funding

Funding to pay the Open Access publication charges for this article was provided by the Engineering and Physical Sciences Research Council (EPSRC).

References

Ammari, H., Buffa, A. & Nédélec, J. C. (2000) A justification of eddy currents model for the Maxwell equations. *SIAM J. Appl. Math.*, **60**, 1805–1823.

Ammari, H., Chen, J., Chen, Z., Volkov, D. & Wang, H. (2014a) Detection and classification from electromagnetic induction data. *J. Comput. Phys.* (submitted). Preprint available at arXiv:1308.6027 [math.AP].

Ammari, H., Chen, J., Chen, Z., Garnier, J. & Volkov, D. (2014b) Target detection and characterization from electromagnetic induction data. *J. Math. Pures Appl.*, **201**, 54–75.

Ammari, H. & Kang, H. (2007) *Polarization and Moment Tensors: With Applications to Inverse Problems*. Berlin, New York, Heidelberg: Springer.

Ammari, H., Vogelius, M. S. & Volkov, D. (2001) Asymptotic formulas for the perturbations in the electromagnetic fields due to the presence of inhomogeneities of small diamater ii. the full Maxwell equations. *J. Math. Pures Appl.*, **80**, 769–814.

Ammari, H. & Volkov, D. (2005) The leading-order term in the asymptotic expansion of the scattering amplitude of a collection of finite number dielectric inhomogeneities of small diameter. *Int. J. Multiscale Comput. Eng.*, **3**, 149–160.

Ao, C., Braunisch, H., O'Neill, K. & Kong, J. (2002) Quasi-magnetostatic solution for a conducting and permeable spheroid with arbitrary excitation. *IEEE Trans. Geosci. Remote Sens.*, **40**, 887–897.

Bachlinger, F., Langer, U. & Schöberl, J. (2005) Numerical analysis of non-linear multiharmonic eddy current problems. *Numer. Math.*, **100**, 594–516.

Bachlinger, F., Langer, U. & Schöberl, J. (2006) Efficient solvers for nonlinear time-periodic eddy current problems. *Comput. Vis. Sci.*, **9**, 197–207.

Baum, C. E. (1971) Some characteristics of electric and magnetic diopole antennas for radiating transient pulses. *Technical Report 125*. Air Force Weapons Laboratory.

Das, Y., McFee, J. E., Toews, J. & Stuart, G. C. (1990) Analysis of an electromagnetic induction detector for real-time location of buired objects. *IEEE Trans. Geosci. Remote Sens.*, **28**, 278–288.

Dassios, G. & Kleinman, R. E. (2000) *Low Frequency Scattering*. Oxford: Oxford Science Publications.

Gaydecki, P., Silva, I., Ferandes, B. & Yu, Z. Z. (2000) A portable inductive scanning system for imaging steel-reinforcing bars embedded within concrete. *Sens. Actuators*, **84**, 25–32.

Griffiths, H. (2005) Magnetic induction tomography. *Electrical Impedance Tomography—Methods, History and Applications* (D. Holder ed.). Bristol, UK: IOP Publishing, pp. 213–238.

Hiptmair, R. (2002) Symmetric coupling for eddy current equations. *SIAM J. Numer. Anal.*, **40**, 41–65.

Jackson, J. D. (1967) *Classical Electrodynamics*. New York: John Wiley and Sons.

Keller, J. B., Kleinman, R. E. & Senior, T. B. A. (1972) Dipole moments in Rayleigh scattering. *J. Inst. Math. Appl.*, **9**, 14–22.

Kleinman, R. E. (1967) Far field scattering at low frequencies. *Appl. Sci. Res.*, **18**, 1–8.

Kleinman, R. E. (1973) Dipole moments and near field potentials. *Appl. Sci. Res.*, **27**, 335–340.

Kleinman, R. E. & Senior, T. B. A. (1982) Rayleigh scattering. *Technical Report RL 728*. University of Michigian Radiation Laboratory.

Ledger, P. D. & Coyle, J. (2005) Evidence of exponential convergence in the computation of Maxwell eigenvalues. *Comput. Methods Appl. Mech. Eng.*, 587–604.

Ledger, P. D. & Lionheart, W. R. B. (2015) The perturbation of electromagnetics fields at distances that are large compared with the object's size. *IMA J. Appl. Math.*, **80**, 865–892.

Ledger, P. D. & Zaglmayr, S. (2010) *hp* finite element simulation of three-dimensional eddy current problems on multiply connected domains. *Comput. Methods Appl. Mech. Eng.*, **199**, 3386–3401.

Marsh, L. A., Ktisis, C., Järvi, A., Armitage, D. & Peyton, A. J. (2013) Three-dimensional object location and inversion of the magnetic polarisability tensor at a single frequency using a walk-through metal detector. *Meas. Sci. Technol.*, **24**, 045102.

Norton, S. J. & Won, I. J. (2001) Identification of buried unexploded ordnance from broadband electromagnetic induction data. *IEEE Trans. Geosci. Remote Sens.*, **39**, 2253–2261.

Pólya, G. & Szegö, G. (1951) *Isoperimetric Inequalities in Mathematical Physics*. Annals of Mathematical Studies, no. 27, Princeton, NJ: Princeton University Press.

Schöberl, J. (1997) NETGEN—an advancing from 2D/3D mesh generator based on abstract rules. *Comput. Vis. Sci.*, **1**, 41–52.

Simmonds, J. & Gaydecki, P. (1999) Defect detection in embedded reinforcing bars and cables using a multi-coil magnetic field sensor. *Meas. Sci. Technol.*, **10**, 640–648.

Smythe, W. R. (1968) *Static and Dynamic Electricity*. New York: McGraw Hill.

Soleimani, M., Lionheart, W. R. B. & Peyton, A. J. (2007) Image reconstruction for high contrast conductivity imaging in mutual induction tomography for industrial applications. *IEEE Trans. Instrumentation Meas.*, **56**, 2024–2032.

Somersalo, E., Isaacson, D. & Cheney, M. (1992) A linearised inverse boundary value problem for Maxwell's equations. *J. Computat. Appl. Math.*, **42**, 123–136.

United Nations (1997). http://www.un.org/cyberschoolbus/banmines/facts.asp. [accessed 26 September 2014].

Wait, R. J. (1953) A conducting permeable sphere in the presence of a coil carrying an oscillating current. *Can. J. Phys.*, **31**, 670–678.

Zaglmayr, S. (2006) High order finite elements for electromagnetic field computation. *Ph.D. thesis*, Institut für Numerische Mathematik, Johannes Kepler Universität, Linz, Austria.

Zaglmayr, S. & Schöberl, J. (2005) High order Nédélec elements with local complete sequence properties. *COMPEL*, **24**, 374–384.

Zolgharni, M., Ledger, P. D., Armitage, D. W., Holder, D. & Griffiths, H. (2009) Imaging cerebral hemorrhage with magnetic induction tomography: numerical modelling. *Physiol. Meas.*, **30**, 187–200.